Short-time dynamics of permeable particles in concentrated suspensions

Gustavo C. Abade, Bogdan Cichocki, Maria L. Ekiel-Jeżewska, Gerhard Nägele, and Eligiusz Wajnryb

Citation: The Journal of Chemical Physics **132**, 014503 (2010); doi: 10.1063/1.3274663
View online: https://doi.org/10.1063/1.3274663
View Table of Contents: http://aip.scitation.org/toc/jcp/132/1
Published by the American Institute of Physics

Short-time dynamics of permeable particles in concentrated suspensions

Gustavo C. Abade,[1] Bogdan Cichocki,[1] Maria L. Ekiel-Jeżewska,[2,a)] Gerhard Nägele,[3] and Eligiusz Wajnryb[2]
[1]*Institute of Theoretical Physics, University of Warsaw, Hoża 69, Warsaw 00-681, Poland*
[2]*Institute of Fundamental Technological Research, Polish Academy of Sciences, Pawińskiego 5B, Warsaw 02-106, Poland*
[3]*Institut für Festkörperforschung, Forschungszentrum Jülich, Jülich D-52425, Germany*

(Received 14 October 2009; accepted 24 November 2009; published online 4 January 2010)

We study short-time diffusion properties of colloidal suspensions of neutral permeable particles. An individual particle is modeled as a solvent-permeable sphere of interaction radius a and uniform permeability k, with the fluid flow inside the particle described by the Debye–Bueche–Brinkman equation, and outside by the Stokes equation. Using a precise multipole method and the corresponding numerical code HYDROMULTIPOLE that account for higher-order hydrodynamic multipole moments, numerical results are presented for the hydrodynamic function, $H(q)$, the short-time self-diffusion coefficient, D_s, the sedimentation coefficient K, the collective diffusion coefficient, D_c, and the principal peak value $H(q_m)$, associated with the short-time cage diffusion coefficient, as functions of porosity and volume fraction. Our results cover the full fluid phase regime. Generic features of the permeable sphere model are discussed. An approximate method by Pusey to determine D_s is shown to agree well with our accurate results. It is found that for a given volume fraction, the wavenumber dependence of a reduced hydrodynamic function can be estimated by a single master curve, independent of the particle permeability, given by the hard-sphere model. The reduced form is obtained by an appropriate shift and rescaling of $H(q)$, parametrized by the self-diffusion and sedimentation coefficients. To improve precision, another reduced hydrodynamic function, $h_m(q)$, is also constructed, now with the self-diffusion coefficient and the peak value, $H(q_m)$, of the hydrodynamic function as the parameters. For wavenumbers $qa>2$, this function is permeability independent to an excellent accuracy. The hydrodynamic function of permeable particles is thus well represented in its q-dependence by a permeability-independent master curve, and three coefficients, D_s, K, and $H(q_m)$, that do depend on the permeability. The master curve and its coefficients are evaluated as functions of concentration and permeability. © *2010 American Institute of Physics*. [doi:10.1063/1.3274663]

I. INTRODUCTION

Hydrodynamic properties of suspensions of permeable colloidal particles moving under creeping flow conditions are of interest not only from a fundamental viewpoint, but also in terms of applications. To gain better control on the industrial processing of colloids in nondilute dispersions requires to understand the hydrodynamic interactions (HIs) between the particles, and their influence on transport properties such as diffusion coefficients or the effective shear viscosity. Examples of permeable colloid suspensions are the so-called fuzzy-sphere systems consisting of permeable particles where the internal structure can change with concentration. A well-studied system of this kind consists of highly permeable, cross-linked polymer network particles (PNiPAM microgel spheres) immersed in an organic solvent. The short-time dynamics of this system has been recently studied by dynamic light scattering.[1] PNiPAM particles are thermosensitive, i.e., they exhibit large and reversible volume changes as a function of temperature.[2–6] In fuzzy particle systems, the suspending fluid can penetrate the particles to an extent depending on the radial distance from the particle center.

Another well-studied class of permeable colloids can be described by a simple core-shell model of spherical particles with a rigid, impermeable spherical core and an outer porous shell. The shell represents the coating of the dry core by some soft material[7–9] such as grafted polymers.[10–16] The coating can stabilize the particles against irreversible aggregation, which otherwise may be induced by the van der Waals attraction in the absence of stabilizing mechanisms. The hydrodynamics in the permeable shell can be described by the Debye–Bueche–Brinkman (DBB) equation for the flow in an isotropic medium of constant porosity k.[17,18] At the outer particle boundary between the bulk fluid and permeable shell, the fluid velocity and hydrodynamic stress change continuously, whereas at the inner particle interface separating the dry core from the permeable shell, stick boundary conditions are commonly used, unless the interface consists mainly of air. In the latter case it is more appropriate to assume zero tangential stress at this interface and zero relative radial velocity.[19]

Notwithstanding the fact that the hydrodynamics of ideal, nonpermeable hard spheres with stick boundary conditions at their surface is different from that of fuzzy and core-shell particles, measurements on permeable particles have

a)Electronic mail: mekiel@ippt.gov.pl.

been commonly interpreted in terms of an effective hard-sphere radius, and an associated effective volume fraction, with values determined to fit the experimental data either for the intrinsic shear viscosity,[20,21] the particle form factor,[21] diffusion coefficients, the static structure factor $S(q)$, or the hydrodynamic function $H(q)$. However, there is no theoretical justification of such a procedure. Moreover, depending on the measured quantity, different values for the effective hard-sphere diameter may be obtained.

The reason why the effective hard-sphere analysis is used so often is that little is known about the HIs in nondilute systems of permeable spheres, in particular, regarding their influence on diffusion transport properties. In contrast with this, colloidal suspensions of impermeable neutral spheres and, to a lesser extent, also impermeable charged spheres have been extensively studied in the past by experiment, theory, and simulation. As a result, the short-time equilibrium transport properties in these systems are now well understood even at high densities (see, e.g., Refs. 22–31).

Note that nonphysical predictions may be made in using an effective hard-sphere interpretation of permeable particles. For instance, the drag force required to push two perfectly smooth hard spheres together along their line of centers at constant relative speed grows without bound near contact, inversely proportional to the gap distance.[32] Different from this, the nonzero slip of fluid at the outer rim of a permeable particle leads to a nonsingular drag coefficient for zero gap width.[33] Thus, two spheres can come in contact during a finite time what has consequences in the aggregation kinetics of unstable colloidal dispersions.[34]

Theory and simulation work on hydrodynamically interacting colloidal porous particles have been concerned so far mostly with the relative motion of two isolated spheres, and the calculation of the associated hydrodynamic drag forces under creeping flow conditions. The two-sphere drag force at finite Reynolds numbers, relevant to large noncolloidal particles not considered here, was calculated by Wu *et al.* using simulations.[35] The axisymmetric and perpendicular migration of multiple core-shell spheres was studied by Chen[33] using a boundary collocation method combined with a lubrication analysis. This study quantified the expected increasing influence of the HIs with decreasing permeability and the finite value of the drag force at particle contact.

Little is known theoretically to date about suspension-averaged transport properties in porous-particle systems, in particular, for nondilute systems. Chen and Cai[36] calculated the mean sedimentation velocity in a homogeneous, monodisperse suspension of uniformly porous spheres to first order in the volume fraction. They showed that the hydrodynamic hindrance effect on the sedimentation coefficient is weakened with increasing permeability, and that the sedimentation velocity is quite sensitive to the direct interactions. For example, addition of a surface charge to the particles strongly reduces the sedimentation coefficient, whereas attractive interactions enhance sedimentation. Mo and Sangani[37] used a multipole expansion method for hydrodynamically interacting porous spheres to obtain numerical results for the average drag force per particle in random and in bcc fixed-bed arrays, and for the high-frequency limiting viscosity of uniformly porous spheres with the equilibrium no-overlap direct interactions. The high-frequency limiting viscosity of a suspension of interacting core-shell particles was also calculated by Russel *et al.*,[38,39] with an account of the density profile of surface-grafted polymers, but with the HIs treated in a lubrication approximation.

On the other hand, there exists an efficient theoretical scheme to calculate HIs in suspensions, based on solving the Stokes equations by the multipole expansion.[40–42] Its advantage in comparison with other formulations of the Stokesian dynamics is that it can be easily modified to account for various hydrodynamic models of the particles. Actually, in the full many-body theoretical algorithm, specific boundary conditions at a particle surface enter only through the single-sphere friction coefficients. Those have been evaluated for a large collection of hydrodynamic models of spherical particles, such as hard spheres with stick boundary conditions, permeable particles, liquid droplets, gas bubbles, particles with slip-stick boundary conditions, and even core-shell particles.[43–47] This theoretical scheme and the corresponding HYDROMULTIPOLE numerical code are therefore well suited to describe the hydrodynamics of a variety of particulate systems. An additional advantage is that, in this approach, higher-order multipole moments are taken into account, resulting in a strictly controlled precision.

The present paper reports on the first comprehensive HYDROMULTIPOLE simulation study of short-time diffusion properties for a suspension of uniformly porous spheres, as a function of the reduced inverse hydrodynamic screening length, $x=a/\sqrt{k}$, and the volume fraction ϕ. For simplicity, and to highlight the generic influence of porosity using a minimal number of system parameters, we assume that spheres of radius a interact directly only via the no-overlap condition. Suspensions at various concentrations are considered, from high volume fractions where many-body HIs are strong, down to dilute systems. Moreover, x is varied from small values representing highly porous particles to very large values where the well-studied limit of nonpermeable hard spheres with stick boundary conditions (hard spheres, for short) is recovered. Using the HYDROMULTIPOLE simulation method, numerical results are derived for the hydrodynamic function $H(q)$ as a function of the scattering wavenumber q, and for the associated short-time diffusion function $D(q)$, probed in dynamic scattering experiments. These two functions reduce at small q to the short-time sedimentation and collective diffusion coefficients, respectively. At large q, both functions asymptote to the short-time (normalized) self-diffusion coefficient. Both sedimentation and self-diffusion coefficients are evaluated numerically by a direct simulation independent of q.

A key finding of the present study is that an appropriately defined *reduced* hydrodynamic function, $h(q)$, is to a good approximation equal to the corresponding reduced function of nonpermeable hard spheres, independent of the permeability. Therefore $H(q)$ can be estimated in terms of a porosity-independent hard-sphere master function, and the limiting values $H(q\to 0)$ and $H(q\to\infty)$, which do depend on the porosity. For $qa\geq 2$, another choice of reduced hydrodynamic function $h_m(q)$ is possible, which allows to express

$H(q)$ with a high precision by a porosity-independent hard-sphere master function and the values of H at the first maximum, $H(q_m)$, and in the limit of large q, $H(q\to\infty)$, which do depend on porosity.

The paper is structured as follows. Section II includes the theoretical background on the short-time dynamics of interacting colloidal spheres and describes our model of porous spheres. The essentials of our multipole method and the simulation procedure are explained in Sec. III. The simulation results, their discussion, and comparison with earlier findings are contained in Sec. IV. The conclusions are given in Sec. V. In Appendix A, we present the single-particle operator of a homogeneously porous sphere used as input in our simulations. A correction used in the extrapolation from a finite-size system to the thermodynamic limit is described in Appendix B. In Appendix C, we discuss the large-wavenumber behavior of the hydrodynamic function and structure factor.

II. SHORT-TIME DYNAMICS

A. General definitions

We consider a macroscopically large system of N equal spherical colloidal particles immersed in a Newtonian, quiescent fluid of shear viscosity η_0. At a low Reynolds number, the fluid velocity field, $\mathbf{v}(\mathbf{r})$, and pressure field, $p(\mathbf{r})$, outside the particles satisfy the stationary Stokes equation[48]

$$\eta_0\nabla^2\mathbf{v}-\nabla p=0,\quad \nabla\cdot\mathbf{v}=0. \tag{1}$$

For a given configuration $\mathbf{X}=\{\mathbf{R}_1,\ldots,\mathbf{R}_N\}$ of centers of freely rotating spheres, the linearity of the hydrodynamic equations leads to a linear relation between the translational particle velocities $\mathbf{U}=\{\mathbf{U}_1,\ldots,\mathbf{U}_N\}$, and the external forces $\mathbf{F}=\{\mathbf{F}_1,\ldots,\mathbf{F}_N\}$ that drive the motion of the spheres:

$$\mathbf{U}_i=\sum_{j=1}^{N}\boldsymbol{\mu}_{ij}^{tt}(\mathbf{X})\cdot\mathbf{F}_j,\quad i=1,\ldots,N. \tag{2}$$

Here, $\boldsymbol{\mu}^{tt}$, with the tensor elements $\boldsymbol{\mu}_{ij}^{tt}$, is the translational-translational part of the mobility matrix. It depends on the configuration of all the particles in the system, and on the hydrodynamic model for the particles.

Short-time colloidal diffusion properties can be probed by a variety of scattering techniques. In photon correlation spectroscopy and neutron spin echo experiments on fluidlike, isotropic systems, the dynamic structure factor, $S(q,t)$, is determined as a function of scattering wavenumber q and correlation time t. On the colloidal short-time scale,[49,50] $S(q,t)$ decays exponentially with time according to

$$\frac{S(q,t)}{S(q)}\approx\exp[-q^2D(q)t], \tag{3}$$

with the q-dependent short-time diffusion function, $D(q)$, defined by the relation,

$$\lim_{t\to0}\frac{\partial}{\partial t}\ln S(q,t)=-q^2D(q). \tag{4}$$

$D(q)$ can be expressed as the ratio

$$D(q)=D_0\frac{H(q)}{S(q)} \tag{5}$$

of the hydrodynamic function $H(q)$, and the equilibrium static structure factor $S(q)=S(q,t=0)$.

The statistical-mechanical expression for $H(q)$ in an infinite isotropic system of mechanically identical colloidal spheres is given by[51]

$$H(q)=\lim_{\infty}\left\langle\frac{k_BT}{ND_0}\sum_{i,j=1}^{N}\exp(i\mathbf{q}\cdot\mathbf{R}_i)\hat{\mathbf{q}}\cdot\boldsymbol{\mu}_{ij}^{tt}(\mathbf{X})\cdot\hat{\mathbf{q}}\exp(-i\mathbf{q}\cdot\mathbf{R}_j)\right\rangle, \tag{6}$$

where $\hat{\mathbf{q}}$ is the unit vector in the direction of $\mathbf{q}$, and the brackets represent an equilibrium ensemble average. Here, $\lim_\infty$ is a short-hand notation for the thermodynamic limit $N\to\infty$, $V\to\infty$, with $n=N/V$ fixed, characterizing a macroscopic system. To shorten the notation, we do not display this limit any more. Whenever an ensemble average is considered in the following, it is tacitly assumed that the thermodynamic limit has been performed.

The positive valued function $H(q)$ has been nondimensionalized by division through the single-particle translational diffusion coefficient, D_0, which is probed experimentally in ultradilute suspensions where detectable interparticle correlations are absent. This coefficient depends on the hydrodynamic model for the particles. In the special case of hard spheres with stick boundary conditions, it is given by $D_0^{\mathrm{hs}}=k_BT/(6\pi\eta_0a)$.

The hydrodynamic function is a measure of the influence of the HIs on short-time diffusion. It consists of a q-independent self-part and a q-dependent distinct-part,

$$H(q)=\frac{D_s}{D_0}+H_d(q). \tag{7}$$

Here, D_s is the short-time translational self-diffusion coefficient for an isotropic system, given on the colloidal short-time scale by the initial slope of the mean-square displacement,[51]

$$D_s=\lim_{t\to0}\frac{1}{6}\frac{d}{dt}\langle[\mathbf{R}_1(t)-\mathbf{R}_1(0)]^2\rangle=\frac{k_BT}{3}\mathrm{tr}\left\langle\frac{1}{N}\sum_{i=1}^{N}\boldsymbol{\mu}_{ii}^{tt}(\mathbf{X})\right\rangle, \tag{8}$$

with tr denoting the trace operation.

In the large-q limit, the distinct part vanishes and $H(q)$ reduces to D_s/D_0. Without HIs, $H(q)$ would be identically equal to one, so that any q-dependence reflects the influence of the HIs. The hydrodynamic function can be interpreted as the (reduced) short-time generalized mean sedimentation velocity in a homogeneous suspension of monodisperse spheres subject to a weak force field collinear with $\mathbf{q}$ and oscillating spatially as $\cos(\mathbf{q}\cdot\mathbf{r})$.[23] Consequently, for $q\to0$, the sedimentation problem in a uniform force field is recovered, so that

$$K = \frac{U}{U_0} = \lim_{q\to 0} H(q) = \frac{k_B T}{3D_0} \mathrm{tr} \left\langle \frac{1}{N} \sum_{i,j=1}^{N} \boldsymbol{\mu}_{ij}^{tt}(\mathbf{X}) \right\rangle_{\mathrm{irr}}, \tag{9}$$

is the concentration-dependent short-time average sedimentation velocity, U, of particles under a uniform force field, normalized by the particle-model dependent sedimentation velocity, U_0, of an isolated particle in the same force field. Because of hydrodynamic long-distance contributions, the limit $q \to 0$ of $H(q)$ is required in the above equation. In the rightmost expression, which does not depend on q, the average is taken with respect to the irreducible part of the mobility tensor, without long-distance contributions.[52] Alternatively, the average can be taken over a periodic cubic cell of size $\mathcal{L}$, in the limit of $\mathcal{L} \to \infty$.

The sedimentation coefficient K can be used for a direct evaluation of the (short-time) collective diffusion coefficient via the expression

$$D_c = \frac{D_0}{S(0)} K = \lim_{q\to 0} D(q), \tag{10}$$

where $S(0) := \lim_{q\to 0} S(q)$ denotes the small-q limit of the static structure factor. In contrast with D_s, which is smaller than D_0 for interacting particles, D_c can be substantially larger than D_0.

Another quantity of interest related to $H(q)$ is the so-called cage diffusion coefficient, defined as the value, $D(q_m)$, of the short-time self-diffusion function $D(q)$ taken at the location q_m of the principal peak in $H(q)$. This peak location coincides practically with that of the principal peak in $S(q)$. It is found empirically that $D(q_m)$ is the minimal value of $D(q)$. The wavelength $2\pi/q_m$ characterizes the size of the next neighbor cage around a particle. For hard spheres this wavelength is roughly equal to the sphere diameter $2a$, and we will see in the following that $q_m a \approx 3$ (independently of volume fraction) also for porous particles.

B. Porous particle model

We assume that the N particles are spheres of the same radius a, consisting of the same uniform material of constant Darcy porosity (permeability) k. For pore sizes sufficiently smaller than a, the flow inside the particles can be described by the Debye-Bueche-Brinkman (DBB) equation

$$\eta_0 \boldsymbol{\nabla}^2 \mathbf{v} - \eta_0 \kappa^2 (\mathbf{v} - \mathbf{u}_i) - \boldsymbol{\nabla} p = 0, \quad \boldsymbol{\nabla} \cdot \mathbf{v} = 0, \tag{11}$$

where $\kappa^{-1} = \sqrt{k}$ is the hydrodynamic screening length, and

$$\mathbf{u}_i(\mathbf{r}) = \mathbf{U}_i + \boldsymbol{\omega}_i \times (\mathbf{r} - \mathbf{R}_i) \tag{12}$$

is the rigid-body velocity field of a sphere i, with center at position $\mathbf{R}_i$, that is moving with translational and rotational velocities $\mathbf{U}_i$ and $\boldsymbol{\omega}_i$, respectively. The DBB equation describes the pore-sized averaged flow inside a porous particle. To determine the colloid diffusion, the Stokes and DBB equations governing the flow outside and inside the spheres, respectively, must be solved under the conditions that the velocity $\mathbf{v}$ and fluid hydrodynamic stress change continuously across the spheres surfaces, and that $\mathbf{v}$ goes to zero far away from the particles. We assume that the particles do not deform and do not overlap.

The mobility tensor in this porous-particle model depends on the reduced inverse hydrodynamic screening length, $x = \kappa a = a/\sqrt{k}$, taken relative to the particle radius a. The single-particle diffusion coefficient, D_0, in the porous sphere model is particularly sensitive to x. We will denote it in the following by $D_0(x)$ to emphasize its x dependence. In the zero permeability limit, $x \to \infty$, the Stokes–Einstein diffusion coefficient, $D_0(\infty) = D_0^{\mathrm{hs}} = k_B T/(6\pi\eta_0 a)$, of an isolated, nonpermeable hard sphere is recovered. The ratio of the hydrodynamic drag on a homogeneously porous sphere relative to that of a nonpermeable one with stick boundary conditions is given by[17,53]

$$\Omega(x) = \frac{D_0^{\mathrm{hs}}}{D_0(x)} = \frac{2x^2(x - \tanh x)}{2x^3 + 3(x - \tanh x)}. \tag{13}$$

The function $\Omega(x)$ grows monotonically from zero to $\Omega(x \gg 1) = 1 - x^{-1} + \mathcal{O}(x^{-2})$ for large x. In terms of $\Omega(x)$, one can define an effective (hard-sphere) hydrodynamic radius of a porous particle, $a_{\mathrm{eff}}(x) = \Omega(x)\ a$. For a highly permeable sphere characterized by a small value of x, $D_0(x)$ is substantially larger than D_0, reflecting the low hydrodynamic friction experienced by a strongly permeable sphere. The coefficient corresponding to $\Omega(x)$ that describes the rotational motion of an isolated, homogeneously porous sphere has been derived in Ref. 54 (see, also Ref. 55). Moreover, the corresponding first-order virial coefficient for the shear viscosity of an ultradilute suspension of uniformly porous spheres in simple shear flow is known since the early work of Debye and Bueche.[17]

While the single-sphere results are well established and have been thoroughly tested experimentally, very little is known about the transport properties of interacting porous spheres. Chen and Cai[36] calculated the first virial coefficient of the sedimentation coefficient, $\alpha_K(x) > 0$, with

$$K(x;\phi) = 1 - \alpha_K(x)\phi + \mathcal{O}(\phi^2), \tag{14}$$

for various values of x. Here, $\phi = (4\pi/3) n a^3$ is the volume fraction for the particle density n. They found that $\alpha_K(x)$ becomes larger with increasing x, in accord with the more general expectation, confirmed by our simulations, that K becomes smaller with increasing x for any value of ϕ, not just small ones. This reflects the growing strength of the HIs for decreasing porosity. It should be born in mind that the enhancement of the mean sedimentation velocity, $U(x;\phi)$, with decreasing x, is due to two contributions: the first one is the enhancement of the single particle sedimentation velocity $U_0(x) \propto D_0(x)$ and the second stems from the decreasing strength of the HIs acting between the particles.

For later use in our discussion, we quote a few analytic results known about the short-time properties of impermeable monodisperse hard spheres. Truncated virial expansion expressions have been derived by Cichocki *et al.*,[56,57]

$$D_s^{\mathrm{hs}}/D_0^{\mathrm{hs}} = 1 - 1.832\phi - 0.219\phi^2 + \mathcal{O}(\phi^3), \tag{15}$$

$$U^{\mathrm{hs}}/U_0^{\mathrm{hs}} = 1 - 6.546\phi + 21.918\phi^2 + \mathcal{O}(\phi^3), \tag{16}$$

$$D_c^{\mathrm{hs}}/D_0^{\mathrm{hs}} = 1 + 1.454\phi - 0.45\phi^2 + \mathcal{O}(\phi^3). \tag{17}$$

The quoted expressions include HIs up to the three-body level and account for lubrication corrections.

For a suspension of nonpermeable hard spheres with arbitrary values of ϕ, numerical results for the sedimentation and diffusion coefficients, and the hydrodynamic function, are known from hydrodynamic force multipole calculations[22] and fluctuating lattice Boltzmann simulations[23–25] pioneered by Ladd, and from the accelerated Stokesian dynamics simulation schemes developed by Brady and co-workers.[26–28] These simulation studies extend up to the freezing volume fraction of hard spheres, partially even up to random closed packing. A comprehensive discussion of the short-time properties of neutral and charge-stabilized hard spheres including many simulation, analytic, and empirical results is given in Ref. 30. The following empirical result is worth mentioning here: The peak height of $H^{\mathrm{hs}}(q)$, attained at $q=q_m$, is given with a good accuracy by the linear form,[30]

$$H^{\mathrm{hs}}(q_m) = 1 - 1.35\phi, \tag{18}$$

valid for concentrations up to the freezing value.

III. MULTIPOLE METHOD

A. Theoretical scheme

In this work, a suspension is modeled by a system of N particles in a periodic cell, with periodic boundary conditions imposed on the flow. For a multipolar description of the HIs between the suspended particles, the fluid flow problem is formulated in the induced force picture,[58–60] where the presence of the particles immersed in the fluid is accounted for by a density $\mathbf{f}_i(\mathbf{r})$ of forces exerted by a particle i on the flow, introduced as a source term in the right hand side of the Stokes Eq. (1) as follows:

$$\eta\nabla^2\mathbf{v} - \nabla p = -\sum_{i=1}^{N} \mathbf{f}_i(\mathbf{r}), \quad \nabla\cdot\mathbf{v} = 0. \tag{19}$$

In this picture, the equations describing the fluid motion are extended to the whole space including the interior of the particles. For a suspension of hard spheres with no-slip boundary conditions, the force density is concentrated on the particle surfaces and the rigid body motion of the particles may be interpreted as a fictitious fluid flow for $|\mathbf{r}-\mathbf{R}_i| \le a$, which satisfies the Stokes Eq. (1). In case of permeable particles the force density is spread throughout the interior of the spheres, in such a way that the DBB Eq. (11) is satisfied, and the fluid velocity and stress are continuous at the particle surface.

If a single particle i, translating and rotating with the local velocity field $\mathbf{u}_i(\mathbf{r})$, specified in Eq. (12), is immersed in an incident fluid flow $\mathbf{v}^{\mathrm{in}}$, it resists the flow, exerting on it the density of forces $\mathbf{f}_i$, which depends linearly on $\mathbf{v}^{\mathrm{in}}-\mathbf{u}_i$ as

$$\mathbf{f}_i = \mathbf{Z}_0(i)(\mathbf{u}_i - \mathbf{v}^{\mathrm{in}}). \tag{20}$$

Here, $\mathbf{Z}_0(i)$ is an integral operator, referred to as the one-particle friction. Its kernel is nonzero only inside the particle volume V_i, including its boundary. The resistance $\mathbf{Z}_0(i)$ depends on the particle porosity and, more generally, on the hydrodynamic model of the interior of the particle and its boundary.

The one-particle friction operator $\mathbf{Z}_0(i)$ and the Green integral operator related to Eq. (19) are the essential quantities needed to evaluate HIs between many particles.[40] In an unbounded system, the fluid flow incident to the particle i is a superposition of an ambient flow $\mathbf{v}_0$, created by external sources in the absence of particles, and the fluid flows generated by all the other particles $j \neq i$,

$$\mathbf{v}^{\mathrm{in}}(\mathbf{r}) = \mathbf{v}_0(\mathbf{r}) + \sum_{j\neq i}^{N} \int \mathbf{T}(\mathbf{r},\mathbf{r}')\cdot\mathbf{f}_j(\mathbf{r}')d\mathbf{r}', \quad \text{for } \mathbf{r}\in V_i \text{ and } \mathbf{r}'\in V_j, \tag{21}$$

where $\mathbf{T}$ is the Green integral kernel for an unbounded fluid, i.e., the Oseen tensor $\mathbf{T}_0$.[48]

The relation (20) for the incident flow (21) can be written in a compact form as

$$\mathbf{f}_i = \mathbf{Z}_0(i)\left[\mathbf{u}_i - \mathbf{v}_0 - \sum_{j\neq i}^{N} \mathbf{G}(ij)\mathbf{f}_j\right], \tag{22}$$

where $\mathbf{G}(ij)$ is an abbreviated notation for the Green operators in Eq. (21), describing the velocity field incident on particle i and induced by a force density on another particle j.

By applying $\mathbf{Z}_0^{-1}(i)$ to both sides of Eq. (22), the following system of integral equations is obtained, each one valid inside a particle volume V_i,

$$\mathbf{u}_i - \mathbf{v}_0 = \sum_{j\neq i}^{N} \mathbf{G}(ij)\mathbf{f}_j + \mathbf{Z}_0^{-1}(i)\mathbf{f}_i, \quad i = 1,\ldots,N. \tag{23}$$

The first contribution on the right hand side of Eq. (23), discussed above, does not depend on a hydrodynamic model of the particles. The second term at the right hand side of Eq. (23) describes the contribution to the velocity of particle i from the induced forces located on the same particle i. This contribution is described in terms of the inverse one-particle friction operator $\mathbf{Z}_0^{-1}(i)$ and it depends on the hydrodynamic model of the particle. For the porous particles investigated in this work, the fluid does not stick to their surfaces and $\mathbf{Z}_0(i)$ is different from the case of hard spheres.

To find the induced force densities, the system of integral Eq. (23) is transformed into an algebraic one by the use of projection on (and expansion in) spherical multipole functions (see Refs. 61–63 for details). The multipole indices l, m, and σ take the values $l=1,2,\cdots$, $m=-l,\ldots,+l$, and $\sigma=0,1,2$. This leads to an algebraic system of equations, written succinctly in the form

$$\mathbf{c} = (\mathbf{Z}_0^{-1} + \mathbf{G})\boldsymbol{f}, \tag{24}$$

where the infinite dimensional vectors $\mathbf{c}$ and $\boldsymbol{f}$ of the velocity and force multipoles consist of the coefficients resulting from the projection of the velocity field $\mathbf{u}_i-\mathbf{v}_0$ and the force density $\mathbf{f}_i$ onto subsequent spherical multipole functions centered at particle $i=1,\ldots,N$. After projecting onto the multipole functions, the operators $\mathbf{Z}_0^{-1}$ and $\mathbf{G}$ become infinite dimensional matrices. Their application to the vector $\boldsymbol{f}$ involves summation over the multipole indices and the particle labels.

The formal solution of Eq. (24) for $\boldsymbol{f}$ is given by

$$\boldsymbol{f} = (\mathbf{Z}_0^{-1} + \mathbf{G})^{-1}\mathbf{c}. \tag{25}$$

Therefore, for porous particles the relation (25) has the same form as for hard spheres, with the same Green function $\mathbf{G}$ but a different single-particle friction $\mathbf{Z}_0$. The multipole elements of $\mathbf{Z}_0$ for porous particles[43,44] are shown explicitly in Appendix A as functions of the permeability.

In numerical computations, the infinite matrices $\mathbf{Z}_0$ and $\mathbf{G}$ are truncated at a multipole order L,[41] such that only elements with $l \leq L$ are taken into account. The truncated matrix $\mathbf{Z}_0^{-1}+\mathbf{G}$ is then inverted, and the force multipoles $\boldsymbol{f}$ are determined. To speed up the convergence of the multipole expansion, the grand friction matrix $(\mathbf{Z}_0^{-1}+\mathbf{G})^{-1}$ is corrected for lubrication effects, which are important if particles are close to each other.[56,64,65] The multipole moments with indices $l=1$ and $\sigma=0$ correspond to the spherical components of forces and translational velocities. Moments with indices $l=1$ and $\sigma=1$ correspond to torques and rotational velocities. The solution of Eq. (25) yields force multipoles of all orders if translational and rotational velocities of the particles and the external flow $\mathbf{v}_0$ are given. The mobility problem of finding translational and rotational velocities for known forces and torques acting on the particles, in the absence of external flow, requires the invertion of the matrix $(\mathbf{Z}_0^{-1}+\mathbf{G})^{-1}$, but only in the space spanned by the multipole functions with indices $l=1$ and $\sigma=\{0,1\}$. According to this procedure,[40] the translational-translational mobility matrices $\boldsymbol{\mu}_{ij}^{tt}$ are evaluated, which are needed to determine the hydrodynamic function.

We emphasize that the single-particle operator $\mathbf{Z}_0$ is the only object that must be changed when different hydrodynamic models for the particle interior and boundary conditions at its surface are considered. The basic Eq. (25) remains the same, and so does the operator $\mathbf{G}$ which, as the propagator of the HIs, depends only on the properties of the suspending fluid and its boundaries. Further insight into the advantages of separating off the single-particle friction may be obtained by expressing the solution of the many-body HIs in terms of the scattering series.[40]

For the periodic system considered in this work, the main structure remains the same as described above for an unbounded fluid. The difference is that for $i \neq j$, the Green operator $\mathbf{G}(ij)$ has now the Hasimoto tensor $\mathbf{T}_H$ (Ref. 66) as its kernel. In addition, there appears a self-part $\mathbf{G}(ii)$, with $\mathbf{T}_H - \mathbf{T}_0$ as its kernel, which accounts for propagation due to all the periodic images.[42] In this approach, the fluid backflow is taken into account in such a way that we are in the frame of reference, in which the suspension velocity, averaged over the periodic cell, is exactly equal to zero.[67] The total force exerted by all the particles on the fluid is compensated by the pressure gradient.

Finally, it is important to point out that, in the mutipole method, the grand friction matrix $(\mathbf{Z}_0^{-1}+\mathbf{G})^{-1}$ is not pairwise additive. We fully take into account many-body HIs between the particles in the periodic cell, without any approximations. Moreover, we apply the lubrication correction, which speeds up the convergence of the multipole expansion and results in a very high accuracy of our computations in the whole range of volume fractions, including very concentrated systems.

B. Numerical computations

The essential steps in the evaluation of HIs, outlined above, have been implemented in the well-established numerical code called HYDROMULTIPOLE;[56] the new element added in this work is the one-particle operator $\mathbf{Z}_0$ for porous particles. Within this scheme, matrix inversions are carried out by use of Cholesky factorization,[68] so that the full N-particle mobility matrix $\boldsymbol{\mu}_{ij}^{tt}$ is evaluated. Then, Eq. (6) is used to determine the hydrodynamic function $H_N(q)$, which is the N-particle counterpart of $H(q)$.

In our computations, the averaging is performed over equilibrium configurations of $N=256$ particles in a periodically replicated cubic simulation cell. This procedure is denoted as $\langle \cdots \rangle_{pbc}$. Equilibrium means here that the N-particle distribution function is equal to one for nonoverlapping particles and zero elsewhere (the standard hard-sphere distribution). A set of independent hard-sphere configurations used in the equilibrium averages for $H(q)$ and U was created using Brownian dynamics simulations and a condensation technique. The results were obtained by averaging over at least 100 independent random configurations for each value of x and ϕ.

The function $H_N(q)$ is calculated for wavenumbers q consistent with the periodic boundary conditions imposed to the simulation cell of length $\mathcal{L}$ and given by the magnitude of the wavevectors $\mathbf{q}=2\pi(n_x,n_y,n_z)/\mathcal{L}$, with the integer n_x, n_y, n_z such that $\sqrt{n_x^2+n_y^2+n_z^2}<45$. The hydrodynamic function $H_N(q)$ is calculated by averaging over the vectors of the same magnitude q. It depends on the number of particles in the periodic cell and needs to be extrapolated to $N \to \infty$.

To allow for simulations of larger systems, with N exceeding 1000, an accelerated version of the HYDROMULTIPOLE code, called FAST HYDROMULTIPOLE, has been developed.[69] In the FAST HYDROMULTIPOLE code, the speed of calculation is improved by applying an iterative method to solve the large system of Eq. (24) for the force multipole moments. Further improvement is achieved by use of the fast multipole algorithm[70] to construct the matrix $\mathbf{G}$ of propagators in sparse form, so that matrix-vector products involving $\mathbf{G}$ require $O(N)$ operations only.

In the fast multipole method, the full mobility matrix $\boldsymbol{\mu}^{tt}$ is not calculated. Instead, the fast method provides the solution of the translational mobility problem in the form of a response velocity vector $\mathbf{U}=\{\mathbf{U}_1,\ldots,\mathbf{U}_N\}$ to applied forces $\mathbf{F}=\{\mathbf{F}_1,\ldots,\mathbf{F}_N\}$. Therefore, the N-particle hydrodynamic function $H_N(q)$ is evaluated according to

$$H_N(q) = \frac{k_B T}{N D_0}\left\langle \sum_{i=1}^{N} \hat{\mathbf{q}} \cdot \mathbf{U}_i(\mathbf{q}) \exp(i\mathbf{q}\cdot\mathbf{R}_i)\right\rangle_{pbc}, \tag{26}$$

where $\mathbf{U}_i(\mathbf{q})$ is the ith particle response to spatially periodic external forces $\mathbf{F}=\{\mathbf{F}_1(\mathbf{q}),\ldots,\mathbf{F}_N(\mathbf{q})\}$ with

$$\mathbf{F}_j(\mathbf{q}) = \hat{\mathbf{q}}\,\exp(-i\mathbf{q}\cdot\mathbf{R}_j). \tag{27}$$

As it has been already mentioned in Sec. II, here we have the picture of $H(q)$ being a short-time generalized sedimentation

coefficient for a homogeneous suspension of monodisperse particles subject to a weak, spatially sinusoidal force collinear with **q**. In particular, the fast-multipole code is very efficient in evaluating the hydrodynamic function at $q=0$, i.e., for the sedimentation coefficient expressed by Eq. (9).

In simulations of homogeneous bulk suspensions, periodic boundary conditions effectively minimize surface effects, but, as the result of long-range HIs, $H_N(q)$ exhibits a strong system-size dependence and measurably deviates from its infinite-system counterpart, $H(q)$, even if N is not small. Simulations are performed for a finite value of N, therefore a finite-size correction from $H_N(q)$ to $H(q)$ has to be evaluated. We extrapolate to the thermodynamic limit using the following expression, valid for $N\to\infty$,

$$H(q) = H_N(q) + 1.76S(q)\frac{\eta_0}{\eta_{\text{eff}}(x,\phi)}(\phi/N)^{1/3}, \tag{28}$$

which, for $q\to 0$ and $q\to\infty$, respectively, includes the finite-size corrections of U and D_s as limiting cases. In this equation, $H_N(q)$ is corrected by a term proportional to $(\phi/N)^{1/3}$. The correction formula was initially proposed by Ladd in the framework of lattice Boltzmann simulations of colloidal hard spheres,[22–24] and subsequently applied successfully to nonpermeable charge-stabilized spheres,[29,30] and in the framework of sedimentation also to porous spheres and drops.[37] It requires as input the static structure factor $S(q)$, and the suspension effective high-frequency shear viscosity $\eta_{\text{eff}}(x,\phi)$.

In this work the structure factor $S(q)$ has been calculated by use of the Verlet–Weis correction to the Percus–Yevick expression (VW-PY).[71,72] The VW-PY expression is specially useful in predicting $S(q)$ in the low-q region, which is inaccessible to simulations of finite systems. Apart from the low-q limit, the structure factor extracted from the hard sphere configurations used in our simulations practically coincides with the VW-PY predictions in the whole range of volume fractions explored.

The suspension effective high-frequency shear viscosity $\eta_{\text{eff}}(x,\phi)$ is evaluated by direct fast-multipole simulations, if ϕ and x are small. For larger ϕ or x, the fast multipole method is used for $N=256,512,1024$ to estimate numerically the slope of the linear dependence of $H(q)$ on $N^{-1/3}$, and to show that it practically does not depend on q. The details of the extrapolation procedure are described in Appendix B. A rigorous theoretical derivation of Eq. (28) is still an open problem, which will be addressed elsewhere.

Finally, we comment on the precision of our simulations. The accuracy of the standard HYDROMULTIPOLE is controlled by changing the multipole truncation order L. As remarked in Refs. 41 and 63, accurate calculations must be performed at least at $L=3$ to account for all long range contributions. Therefore, generically we use $L=3$. The accuracy of the FAST HYDROMULTIPOLE is controlled by L and by an additional truncation order L' $(\geq L)$, discussed in Ref. 69. To evaluate the extrapolation $N\to\infty$, we truncate the multipole expansions at $L=3$ and $L'=3$.

For small wavenumbers q, large x and large volume fractions ϕ, precision of the Cholesky multipole method with the truncation at $L=3$ deteriorates up to 10% and an extrapolation to larger values of L is needed. First, the hydrodynamic function is evaluated by the fast-multipole method with $L=3,5$ for $N=64,256$ particles in the periodic cell and it is shown that the ratio of values corresponding to $L=3$ and $L=5$ very weakly depends on N. Next, computations are performed with the Cholesky method for $L=3,4,5,6$ at a smaller number of particles $N=64$. It is found that $L=6$ is sufficient, because it gives practically the same results as $L=5$. Then, we calculate the ratio of the $H(q)$-values at $L=3$ and $L=6$, and we use it to extrapolate from $L=3$ to $L=6$ all the data previously obtained for the hydrodynamic function $H(q)$. The resulting accuracy of the multipole truncation is better than 1% at low values of q, and better than 0.5% for moderate and large values of q.

Summarizing, we proceed as follows:

(i) Compute the finite-system function $H_N(q)$ by the Cholesky multipole method with periodic boundary conditions; ensemble average over equilibrium configurations of nonoverlapping particles.
(ii) Calculate the infinite-system function $H(q)$ by correcting $H_N(q)$ for implicit finite-size effects with the fast-multipole method, as described in Appendix B.
(iii) Correct for the multipole truncation to reach an accuracy not worse than 1% at low q and not worse than 0.5% at larger wavenumbers.

IV. RESULTS

We present simulation results for $H(q)$, and for the self-diffusion and sedimentation coefficients of porous spheres using inverse permeabilities $x=3$, 5, 10, 30, 50, 100, and ∞ (hard spheres), and volume fractions in the fluid regime selected as $\phi=0.05$, 0.15, 0.25, 0.35, and 0.45. The results have been obtained using the method and procedures described in the previous section. Recall that the quantities introduced in Sec. II have been nondimensionalized by division through the infinite-dilution single-particle diffusion coefficient D_0. For the present model of uniformly permeable spheres, $D_0(x)$ is a function of the single parameter x that quantifies the degree of permeability. In Table I, $D_0(x)$ is compared with the hard-sphere analog, D_0^{hs}, by listing the single-sphere reduced drag coefficient, $\Omega(x)=D_0^{\text{hs}}/D_0(x)$, evaluated according to Eq. (13), for the permeabilities considered in our simulations. This table illustrates the basic hydrodynamic behavior of the porous particles with the specific values of x used in our simulations. We recall that $\Omega(x)$ is the effective hydrodynamic radius of the porous particle, measured relative to its geometric radius a. In typical experimental systems of core-shell particles with a thick permeable shell of grafted polymer chains, $x\sim 20-30$.[15]

TABLE I. Single-sphere reduced drag coefficient, $\Omega(x)=D_0^{\text{hs}}/D_0(x)$, quoted in Eq. (13).

x	3	5	10	30	50	100	∞
$\Omega(x)$	0.6013	0.7634	0.8880	0.9651	0.9794	0.9899	1.0000

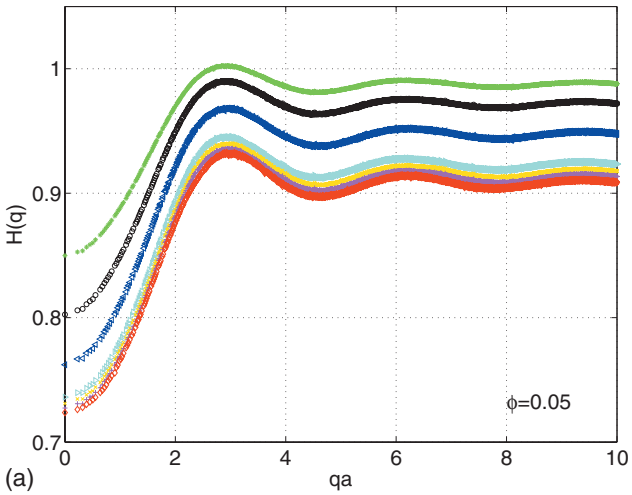

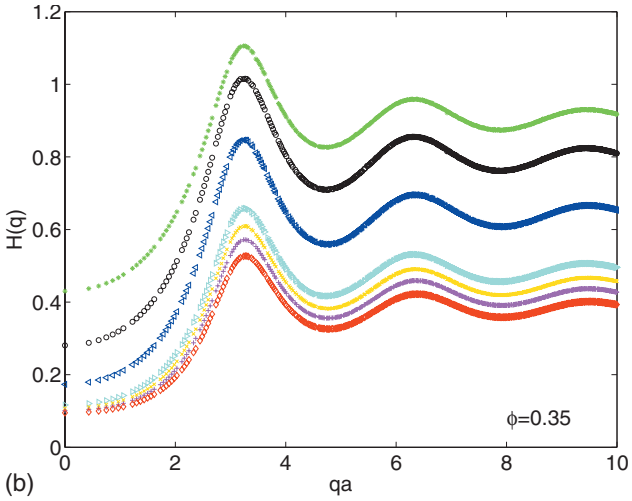

FIG. 1. Simulation results for the hydrodynamic function $H(q)$ for $x=3,5,10,30,50,100,\infty$ (from top to down). Top figure: $\phi=0.05$. Bottom figure: $\phi=0.35$.

A. Hydrodynamic function

In Fig. 1, our simulation results for the hydrodynamic function, $H(q)$, are displayed for various values of the reduced inverse hydrodynamic screening length x, for a dilute and an intermediately concentrated system. With increasing x, i.e., decreasing permeability, and a fixed value of ϕ, $H(q)$ becomes smaller for all values of q. This reflects the decrease in the generalized, q-dependent sedimentation coefficient $H(q)$ when the strength of the HIs is increased by making the particles less permeable. We further notice from this figure that changing x does not affect the location, q_m, of the principal peak in $H(q)$. The principal peak location, q_m, coincides practically with that of the static structure factor. The latter location is independent of the HIs since $S(q)$ is a genuine static equilibrium property. Notice further that the oscillations in $H(q)$ become stronger with increasing concentration.

Whereas both $H(q \ll q_m) \approx K$ and $H(q \gg q_m) \approx D_s/D_0$ decrease with increasing ϕ, for any value of x, documenting thus the expected decline of the sedimentation and self-diffusion coefficients with increasing concentration, the ϕ-dependence of $H(q_m)$ changes qualitatively as a function of x, as shown in Fig. 2 and Table II. For highly permeable

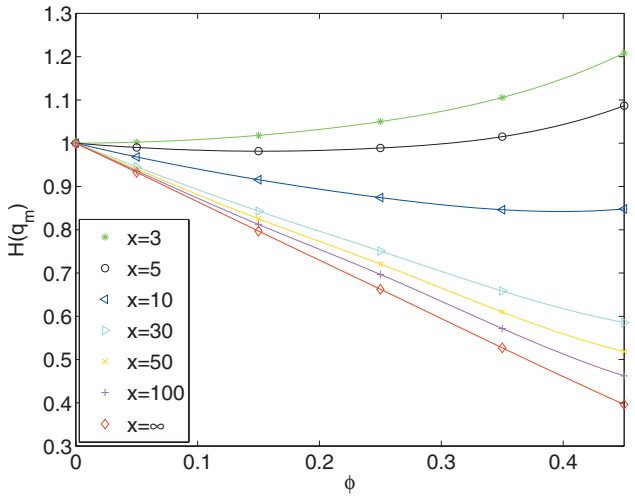

FIG. 2. Hydrodynamic function principal peak value, $H(q_m)$, as a function of volume fraction, for various permeabilities as indicated. The simulation points are linked by spline fits to guide the eye.

particles where $x \leq 3$, $H(q_m)$ increases monotonically with increasing ϕ, akin to what is observed in dilute, low-salinity suspensions of strongly charged, nonporous spheres.[29] For $x \approx 5-10$, there is even a small nonmonotonicity observable in the density dependence. At larger permeabilities $x \geq 20$, $H(q_m)$ declines monotonically in ϕ. The strongest decline takes place for $x \to \infty$. This decline agrees very well with the linear density form quoted in Eq. (18) with the same coefficient 1.35.

B. Reduced hydrodynamic functions

Consider the *reduced* hydrodynamic function

$$h(q) = \frac{H(q) - H(\infty)}{H(\infty) - H(0)}, \tag{29}$$

with $H(\infty)=D_s/D_0$ and $H(0)=K$. It is defined such that $h(q \to \infty)=0$ and $h(q \to 0)=-1$, with its overall q dependence resembling that of the original $H(q)$. Notice here also that $h(q)=H_d(q)/|H_d(0)|$, where $H_d(q)$ is the distinct part of the hydrodynamic function introduced in Eq. (7). It should be kept in mind that $h(q)$ is also a function of ϕ and x. In general, $D_s/D_0 > K$ for nonzero ϕ, so that $h(q)$ is positive whenever $H(q)-D_s/D_0=H_d(q)>0$. Our numerical results for $h(q)$, covering the range from highly porous to nonpermeable spheres with stick boundary conditions, and from

TABLE II. Principal peak value, $H(q_m)$, of hydrodynamic function for different values of x and ϕ.

	ϕ				
x	0.05	0.15	0.25	0.35	0.45
3	1.002	1.018	1.050	1.106	1.208
5	0.990	0.982	0.989	1.015	1.087
10	0.968	0.916	0.874	0.846	0.848
30	0.946	0.843	0.751	0.658	0.586
50	0.940	0.825	0.721	0.610	0.519
100	0.936	0.812	0.697	0.572	0.462
∞	0.933	0.797	0.663	0.527	0.396

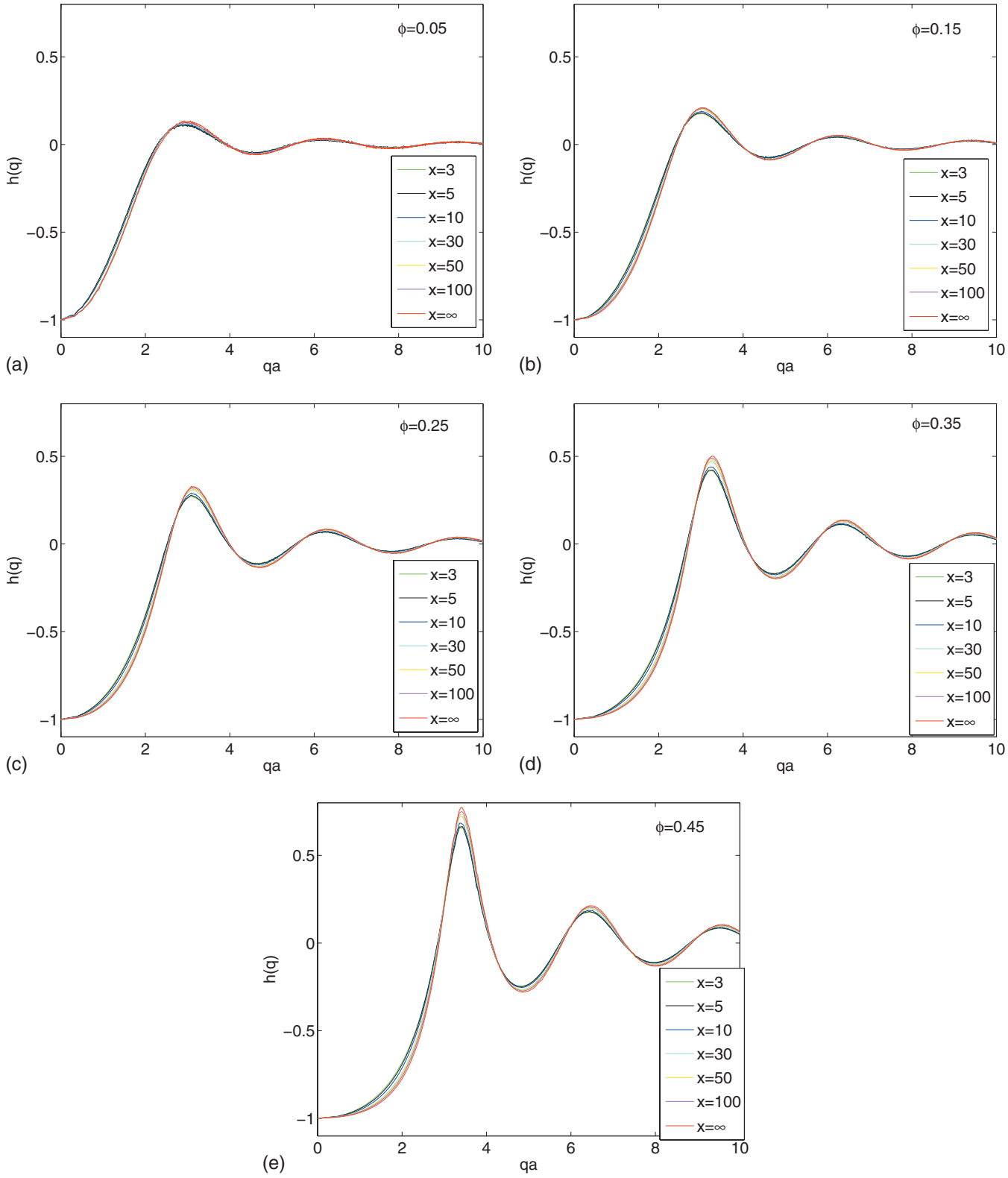

FIG. 3. Reduced hydrodynamic function $h(q)$, for values of x and ϕ as indicated.

dilute to concentrated systems, are displayed in Fig. 3.

The first key finding in our study, demonstrated by this figure, is that $h(q)$ remains nearly independent of the permeability for all values of q. There are some slight variations in $h(q)$ when x is changed, and these are most visible in the amplitudes of the oscillations in $h(q)$ that grow with increasing x, and also in the small-q region located to the left of the principal peak in $h(q)$. The principal peak, $h(q_m)$, of $h(q)$ attains its largest value when $x \to \infty$.

Since $h(q)$ is only weakly dependent on x, it can be approximated by the hard-sphere reduced hydrodynamic function,

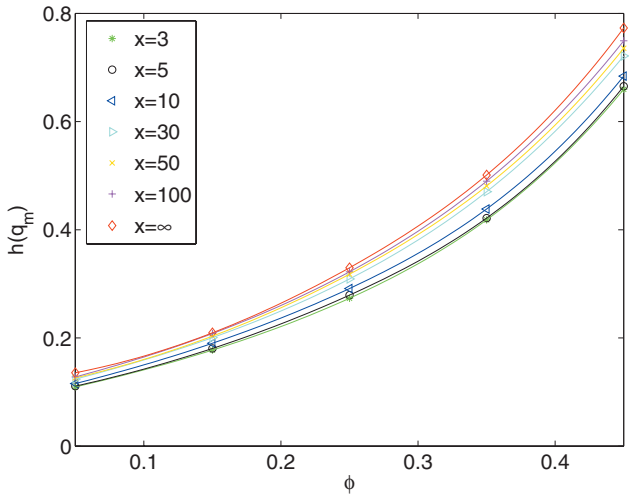

FIG. 4. Reduced hydrodynamic function principal peak value, $h(q_m)$, as a function of volume fraction, for various permeabilities as indicated. The simulation points are linked by spline fits to guide the eye.

$$h(q) \approx h^{\mathrm{hs}}(q). \tag{30}$$

Accordingly, the hydrodynamic function is well approximated by

$$H(q;x) \approx \left(\frac{D_s(x)}{D_0(x)} - K(x)\right) h^{\mathrm{hs}}(q) + \frac{D_s(x)}{D_0(x)}, \tag{31}$$

where the additional ϕ-dependence of the various quantities has not been displayed for brevity. While we confirmed the very weak dependence on x explicitly for uniformly permeable spheres only, we expect that the dependence of $h(q)$ on permeability remains very weak also for a more complex hydrodynamic structure of a particle, such as for the core-shell model.

Recall that the common principal-peak location, q_m, of $H(q)$ and $h(q)$ is practically that of the $S(q)$ of hard spheres, so that it is independent of the permeability. Quite remarkable is the low x-sensitivity of the peak value, $h(q_m)$, of the reduced hydrodynamic function $h(q)$, in particular, since the peak, $H(q_m)$, of the original $H(q)$ varies strongly with x (see again Fig. 2). The explicit dependence of $h(q_m)$ on ϕ and x is shown in Fig. 4. In the wide range of considered porosities, $3 \leq x \leq \infty$, the value of $h(q_m)$ changes by less than 20%.

A careful analysis of our results for $h(q)$ in Fig. 3 suggests that a more accurate description can be obtained if a second reduced hydrodynamic function, $h_m(q)$, is introduced, now with the use of $H(q_m)$ rather than $H(0)$,

$$h_m(q) = \frac{H(q) - H(\infty)}{H(q_m) - H(\infty)} = \frac{H_d(q)}{H_d(q_m)}. \tag{32}$$

By definition, $h_m(q_m)=1$, independently of x and ϕ. Figure 5 demonstrates that for wavenumbers $qa > 2$, including the principal peak region of the hydrodynamic function, $h_m(q)$ is insensitive to x. A significant x-dependence is observed only at small-q values near to and in the hydrodynamic regime, where $H(q) \approx K$. The coefficient K depends strongly on x, as it will be discussed in the next section.

We have here the remarkable finding that for $qa > 2$, the hydrodynamic function $H(q)$ is determined with a high precision by its principal peak value, $H(q_m)$, and $H(\infty)=D_s/D_0$, with the q-dependence characterized by $h_m^{\mathrm{hs}}(q)$. Explicitly,

$$H(q;x) \approx \left(H(q_m;x) - \frac{D_s(x)}{D_0(x)}\right) h_m^{\mathrm{hs}}(q) + \frac{D_s(x)}{D_0(x)}, \quad \text{for} \quad qa > 2. \tag{33}$$

We note finally that the oscillations in $H(q)$, and in the associated reduced functions $h(q)$ and $h_m(q)$, are growing with increasing particle concentration.

C. Hydrodynamic function at low wavenumbers

After completing the analysis of the hydrodynamic function for wavenumbers $qa \geq 2$, we now focus on small wavenumbers, $qa \leq 2$. We start with $q=0$, in evaluating the sedimentation and collective diffusion coefficients. Table III includes our numerical results for the sedimentation coefficient $K(x;\phi)$. The plots are given in Fig. 6(top).

Since the major effect of permeability is to weaken the HIs, K decreases faster with increasing concentration when the permeability is decreased. Nonpermeable spheres sediment most slowly, for the two reasons that the influence of the HIs is strongest, and that the single-particle diffusion coefficient is smaller than for permeable ones. The ϕ-dependence of K, for $x=\infty$, agrees well with earlier results for the sedimentation coefficient of nonpermeable hard spheres obtained by Ladd using a force multipole method.[22] From Eq. (16) for hard spheres, it follows that $\mathcal{O}(\phi^2)$ corrections are contributing significantly already for $\phi=0.05$. For this reason, the simulation points in the figure have been connected by solid lines using a spline fit. The slopes of the solid lines for $x=\infty$ and $x=10$ agree well with the dashed lines, corresponding to the first-order virial results for $x=\infty$ and $x=10$ derived by Batchelor[73] and Chen and Cai,[36] respectively.

The normalized collective diffusion coefficient, D_c/D_0, follows from Eq. (10), if K is divided by $S(0)$, with the latter given with a high accuracy by the Carnahan–Starling analytic expression, $S(0)=(1-\phi)^4/[(1+2\phi)^2+\phi^3(\phi-4)]$. The result is plotted in Fig. 6(bottom). Notice the weak ϕ-dependence of D_c for nonpermeable spheres.

Since $S(0)$ in our model is independent of x, the monotonic rise of D_c/D_0 with increasing ϕ is more pronounced for more permeable particles. We point out that D_c depicted in Fig. 6(bottom) is a short-time quantity which at larger

TABLE III. Sedimentation coefficient K as a function of x and ϕ.

	ϕ				
x	0.05	0.15	0.25	0.35	0.45
3	0.850	0.641	0.511	0.430	0.378
5	0.803	0.536	0.376	0.281	0.221
10	0.762	0.452	0.275	0.173	0.114
30	0.736	0.399	0.217	0.117	0.0618
50	0.731	0.389	0.206	0.108	0.0542
100	0.727	0.382	0.199	0.101	0.0492
∞	0.724	0.377	0.192	0.0949	0.0448

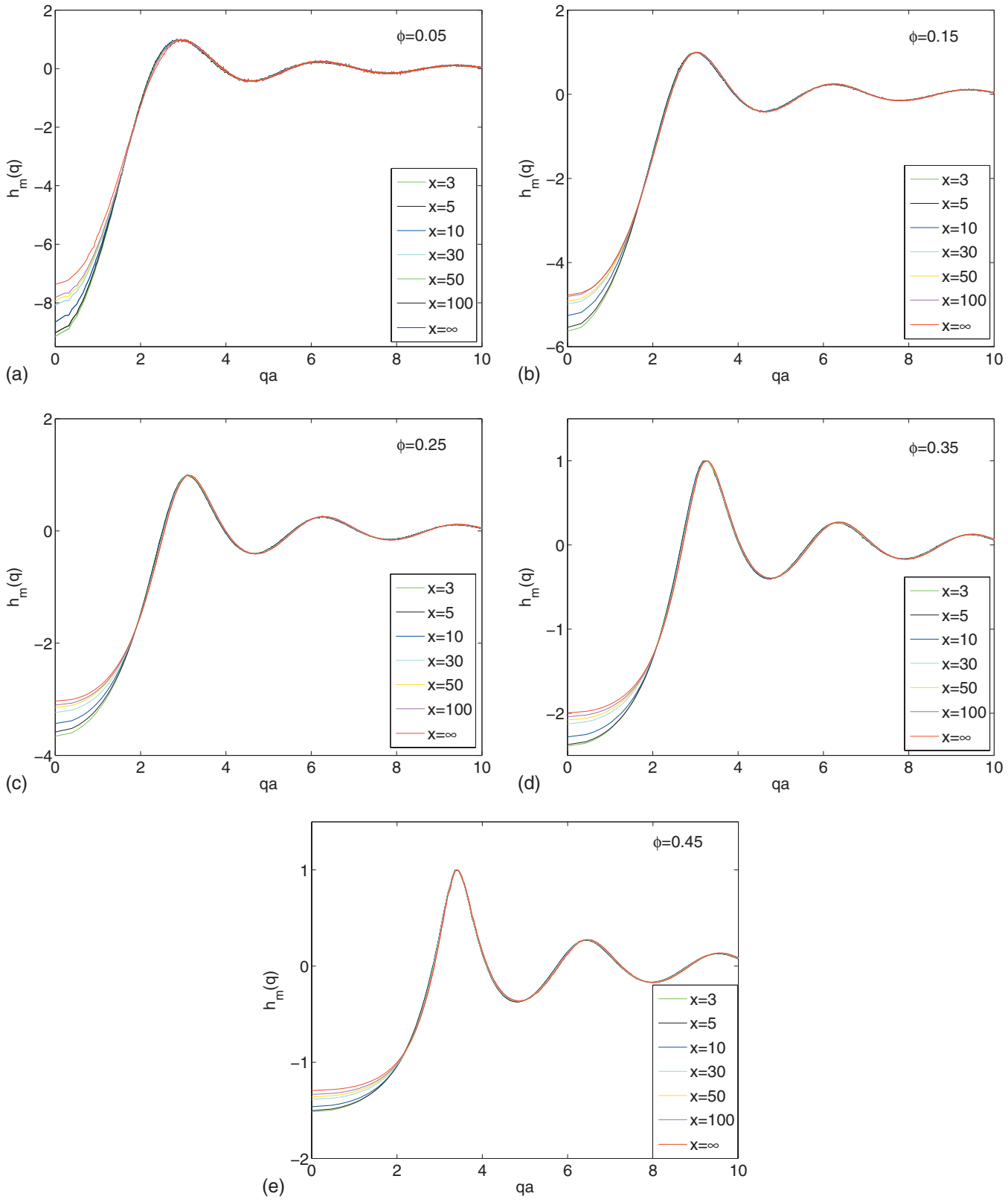

FIG. 5. Reduced hydrodynamic function, $h_m(q)$, for values of x and ϕ specified in the plots.

concentrations, where many-body HIs are active, should be distinguished from the long-time collective diffusion coefficient. The latter is affected by memory (dynamic caging) effects and is also referred to as gradient diffusion coefficient measurable in a macroscopic diffusion experiment. The values taken by the long-time coefficient in dense systems are smaller than the ones for D_c, but the difference is commonly quite small.[74]

For small wavenumbers, $qa \leq 2$, the reduced hydrodynamic function $h_m(q)$ deviates by up to 20% from the hard-

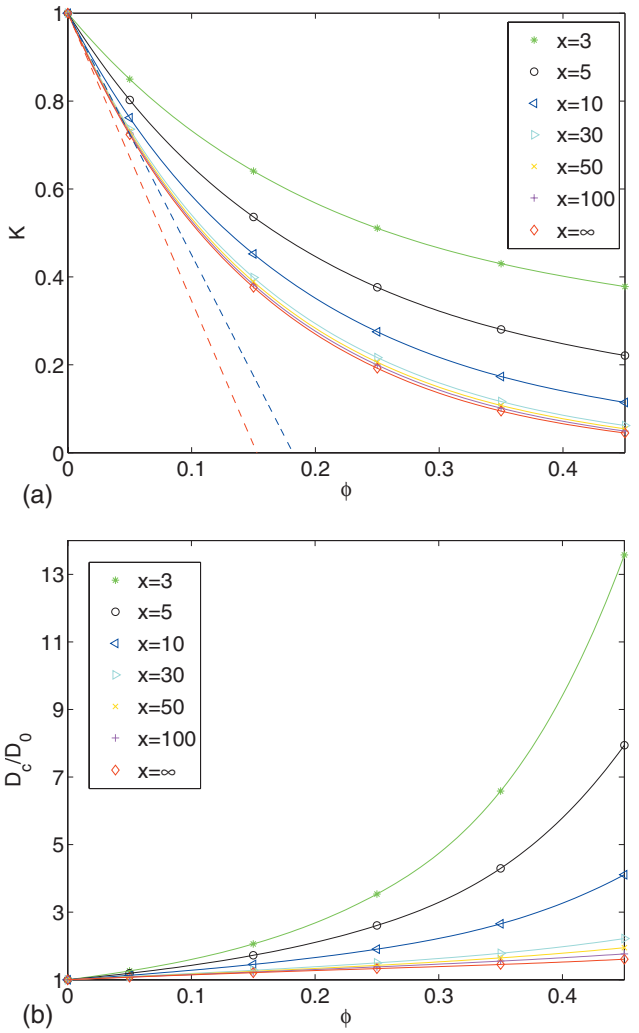

FIG. 6. Sedimentation coefficient (top) and collective diffusion coefficient (bottom) as a function of volume fraction for different permeabilities as indicated. The simulation points are connected by spline fits. The dashed red and blue straight lines are, respectively, the first-order virial expansion results for nonpermeable hard spheres, $K^{hs}=1-6.546\phi$ (Ref. 73), and strongly permeable particles where $K=1-5.5\phi$, for $x=10$ (Ref. 36).

TABLE IV. Coefficients A and B in Eq. (34), as functions of x and ϕ.

	ϕ				
x	0.05	0.15	0.25	0.35	0.45
			A		
3	2.74	1.07	0.43	0.178	0.076
5	2.68	1.01	0.39	0.165	0.069
10	2.45	0.89	0.34	0.139	0.056
30	2.06	0.74	0.27	0.105	0.043
50	1.97	0.70	0.24	0.093	0.039
100	1.91	0.66	0.22	0.084	0.036
∞	1.79	0.61	0.20	0.076	0.029
			B		
3	−0.184	0.000	0.031	0.021	0.011
5	−0.178	0.007	0.033	0.022	0.012
10	−0.144	0.022	0.038	0.023	0.012
30	−0.084	0.037	0.042	0.023	0.011
50	−0.072	0.043	0.043	0.024	0.011
100	−0.062	0.046	0.044	0.023	0.011
∞	−0.060	0.055	0.046	0.023	0.011

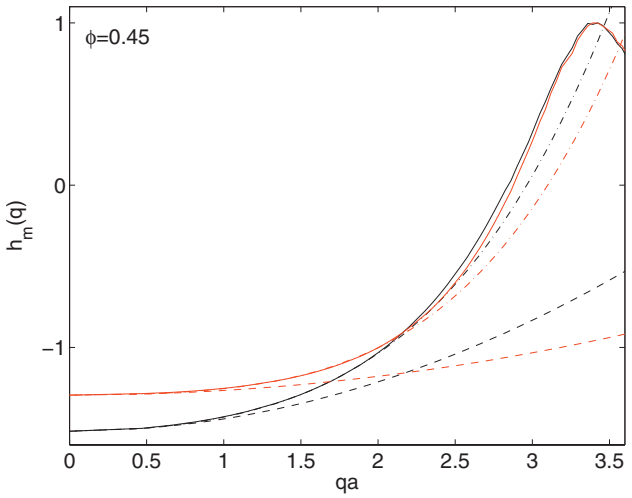

FIG. 7. Low-wavenumber dependence of the reduced hydrodynamic function $h_m(q)$ at $\phi=0.45$, for permeable particles with $x=3$ (black solid line) and hard spheres with $x=\infty$ (red solid line), in comparison with the polynomial approximation in Eq. (34). The approximation $h_m(0)+A(qa)^2$ (dashed lines) is sufficient for $qa\leq 1$. For $qa\leq 2$, the term $(qa)^4$ has to be taken into account (dashed-dotted lines).

sphere master curve when x is decreased down to $x=3$, as shown in Fig. 5. The q-dependence of $h_m(q)$ in this range will now be discussed. For $qa\leq 1$, it is well approximated by $h_m(q)=h_m(0)+A(qa)^2$, with the coefficient A given in Table IV for different ϕ and x. As illustrated in Fig. 7, for $1\leq qa\leq 2$ the linear approximation in $(qa)^2$ is not sufficient, but $h_m(q)$ is well approximated if also the $(qa)^4$ term is taken into account,

$$h_m(q) \approx h_m(0) + A(qa)^2 + B(qa)^4. \tag{34}$$

Values for the coefficient B are listed in Table IV. For a larger volume fraction, $\phi\geq 0.35$, B is practically independent of x.

D. Self-diffusion coefficient

In our simulations, D_s/D_0 is determined by calculating the trace of the translational-translational mobility matrix ac-

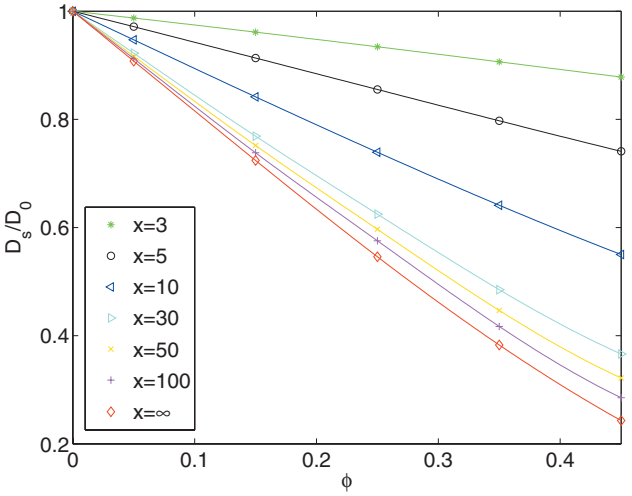

FIG. 8. Self-diffusion coefficient, D_s/D_0, for permeabilities as indicated. The simulation points are connected by spline fits to guide the eye.

TABLE V. Self-diffusion coefficient D_s/D_0 as a function of x and ϕ.

	ϕ				
x	0.05	0.15	0.25	0.35	0.45
3	0.987	0.961	0.934	0.906	0.878
5	0.971	0.913	0.855	0.797	0.741
10	0.947	0.842	0.739	0.641	0.550
30	0.922	0.769	0.625	0.485	0.367
50	0.917	0.752	0.597	0.447	0.322
100	0.912	0.738	0.576	0.417	0.285
∞	0.908	0.724	0.546	0.383	0.243

cording to Eq. (8). The results are documented in Fig. 8 and Table V. As one notices from Fig. 8, D_s/D_0 decays monotonically in ϕ, and its decay is faster for less permeable spheres. The ϕ-dependence of $D_s(x=\infty)$ agrees well with earlier data gained by other numerical methods.[22,26,30]

The precise values of D_s/D_0 listed in Table V are used now to discuss the accuracy of alternative ways of estimating the self-diffusion coefficient, which are of help to extract D_s/D_0 from experimental data. Suppose that, in a scattering experiment, $H(q)$ is measured up to, say, $qa \leq 8$, which is roughly the location of its third minimum. Then, D_s can be accurately determined by a least-squares fit of the large-q asymptotic form of $H(q)$, to the data of $H(q)$, in the range, e.g., of $4 \leq qa \leq 8$. Details of this method are given in Appendix C. With this procedure, D_s/D_0 is determined with an absolute error of 0.001 or smaller.

Pusey[75] suggested and underpinned experimentally that self-diffusion can be probed in a dynamic light scattering experiment performed at wavenumbers, $q^* > q_m$, where $S(q^*)=1$, on assuming that $D_s \approx D(q^*)$ is valid approximately. In a light scattering experiment, the smallest of these q^* (denoted as q_1^*) is usually attainable. In Appendix C, it is explained that this approximation works well, since $H(q)$ and $S(q)$ share a similar large-q asymptotic form, differing only in the expansion coefficients. Asymptotic considerations are also used to estimate the accuracy of the approximation.

Using the HYDROMULTIPOLE code, we demonstrated that Pusey's method to determine self-diffusion is efficient also for permeable particles, for any degree of permeability, when q_1^* or the next larger q^* (denoted as q_2^*) are used. This can be seen from Table VI which includes values for D_s/D_0 obtained by direct simulation based on Eq. (8), together with the corresponding estimates for the self-diffusion coefficient by $H(q_1^*)$ and $H(q_2^*)$, respectively. The estimate for D_s/D_0 given by $H(q_1^*)$ differs from the directly calculated values by no more than 6%. The higher error is found for the larger ϕ and x. The differences shrink to a mere 1% or less when $H(q_2^*)$ is used as estimate. While both estimates are useful in measuring self-diffusion, sensitive light scattering measurements at q_2^* are much harder to achieve than those for the smaller wavenumber q_1^*.

The accuracy of Pusey's approximation, $D_s \approx D(q_1^*)$, has been recently also tested[30] for nonpermeable hard spheres and charge-stabilized spheres, using Stokesian dynamics computer simulations both of D_s and $H(q_1^*)$. For all systems explored in Ref. 30, the difference between D_s/D_0 and $H(q_1^*)=D(q_1^*)/D_0$ was found to be less than 10%.

TABLE VI. Comparison of the self-diffusion coefficient D_s/D_0 and its approximations $H(q_1^*)$ and $H(q_2^*)$.

	Method		
x	D_s/D_0	$H(q_1^*)$	$H(q_2^*)$
	$\phi=0.15$		
3	0.961	0.961	0.962
5	0.913	0.914	0.914
10	0.842	0.843	0.842
30	0.769	0.771	0.768
50	0.752	0.754	0.751
100	0.738	0.741	0.737
∞	0.724	0.727	0.722
	$\phi=0.45$		
3	0.878	0.899	0.886
5	0.741	0.762	0.749
10	0.550	0.568	0.556
30	0.366	0.381	0.368
50	0.322	0.336	0.323
100	0.285	0.300	0.285
∞	0.243	0.257	0.242

V. CONCLUSIONS

Using the model of uniformly permeable spheres, a comprehensive simulation study was made on short-time diffusion properties of suspensions of permeable hard spheres, where the fluid can permeate inside the particles and move relative to their rigid skeleton. Our study covers the fluid-phase concentration range. Permeabilities were analyzed in the full span from impermeable to strongly permeable particles. The simulation data for the hydrodynamic function extend over a wide range of wavenumbers including the third peak. The results for $H(q)$, sedimentation coefficient K, and self-diffusion coefficient D_s have been obtained by a versatile hydrodynamic multipole method, encoded in the program package HYDROMULTIPOLE of a strictly controlled, high precision. The most important result of the present study is that the q-dependence of $H(q)$ can be mapped to good accuracy to that of impermeable hard spheres. In contrast with this, the limiting large-q and small-q values of $H(q)$, i.e., D_s/D_0 and K, do strongly depend on the permeability. Both quantities increase with increasing permeability, in particular, at higher concentrations, since the flow of fluid inside the particles relative to their skeletons leads to a reduction in both of the HIs and the single-particle hydrodynamic friction. Raising the permeability leads to an upward shift of $H(q)$ for all values of q. The principal peak height, $H(q_m)$, of the hydrodynamic function which is related to the cage diffusion coefficient is also found to depend strongly on x. The volume concentration dependence of the peak value changes even in a qualitative way from a monotonic decay for intermediately small permeabilities ($x > 10$), to a monotonic increase at high permeabilities $x \leq 3$, and a slightly nonmonotonic concentration dependence in between (for $x \sim 5-10$).

Two forms of a reduced hydrodynamic function, namely, $h(q)$ and $h_m(q)$, have been discussed. The function $h(q)$ is defined as the distinct hydrodynamic function, $H_d(q)$, divided by its absolute value taken at zero wavenumber. It is only very weakly x-dependent for all values of q, with the residual x-dependence most visible close to the peak locations. The reduced hydrodynamic function, $h_m(q)$, is defined as $H_d(q)$ divided by $H_d(q_m)$. The function $h_m(q)$ is practically permeability independent for all wavenumbers $q>2$, including the principal peak region.

Therefore the shape of the hydrodynamic function for permeable particles is determined by the $H(q)$ for nonpermeable hard spheres. We therefore deduce the most important conclusion of this work: the essential information about the hydrodynamic structure of particles is contained only in the sedimentation, self-diffusion, and also cage-diffusion coefficients. Therefore, measurements of these quantities can be used to verify the internal structure of the suspension particles and the behavior of the fluid velocity and stress at their surfaces.

Our findings on the behavior of the reduced hydrodynamic functions show that any attempt to understand (short-time) transport properties of permeable particles simply in terms of an effective radius ($a \rightarrow a_{\mathrm{eff}}$) will not lead to satisfactory results, since the expressions in Eqs. (31) and (33) relating $H(q)$ to its reduced functions cannot be mapped onto a single effective radius. The reduction procedure shifts and scales *values* of the hydrodynamic function, but does not change its *argument* qa. The effective-radius concept for permeable particles has thus no theoretical justification. This agrees with the general conclusions drawn from hydrodynamic function measurements on PNiPAM microgel spheres in dimethylformamide,[1] and core-shell particles with a hard silica core and a soft polymeric shell,[7] that $H(q)$ cannot be described properly using the effective hard-sphere model of nonpermeable spheres. Aside from that, we note that permeability cannot explain the astonishingly small hydrodynamic functions purportedly measured[76] for low-salinity suspensions of smaller-sized charge-stabilized colloidal spheres, with values for $H(q)$ substantially smaller than even those of neutral, impermeable hard spheres. On the contrary, as discussed above for neutral spheres, a nonzero permeability leads to an upward shift of $H(q)$. This should apply also to charged spheres, as shown in Ref. 36 for the special case of sedimentation. A critical discussion of the findings in Ref. 76 is given in Ref. 29.

We discussed various ways to determine the (short-time) self-diffusion coefficient, D_s, of permeable particles. The most convenient way is Pusey's method where $D(q)$ is measured at the smallest wavenumber $q>q_m$ such that $S(q)=1$. According to our study, a decent estimate of D_s is obtained in this way with at most a few percent of inaccuracy. A high precision value for D_s with less than one percent deviation follows from identifying it with $D(q)$ at the next larger wavenumber $q>q_m$ for which $S(q)=1$, of course provided that a sufficiently accurate scattering measurement can be performed at such a large wavenumber.

The predictions of our study can be verified by dynamic light or synchrotron radiation measurements of $S(q,t)$ for a concentration series of sterically stabilized particle systems of varying (overall) permeability. In addition, our results can serve as a database for experimentalists working on the dynamics of neutral porous colloidal particles and aggregates. The generic trends found for the short-time transport properties of uniformly porous spheres, in particular the weakening of the HIs with increasing permeability, can be expected to remain valid for more complex hydrodynamic particle structures. An important example with a wide range of applications is the core-shell model describing particles with one or more porous layers around an impermeable core. Numerical work on transport properties of core-shell particle suspensions is in progress and will be documented in a future publication.

In this paper, we restricted ourselves to the short-time regime. In this regime, HIs have no influence on distribution of particles which is the thermodynamic equilibrium one. The hard-sphere model of interaction between the suspended particles is the simplest. But our codes allow to treat more complicated, and in many cases more realistic, interparticle direct interactions. The short-time regime, analyzed in this work, is very interesting for experimentalists. However, they also perform measurements for long times. In this case HIs influence the structure of a suspension. With our FASTHYDROMULTIPOLE code we are able to perform appropriate simulations to create an ensemble of particle trajectories and next to calculate long-time suspension transport coefficients. This will be a subject of one of our future works.

Finally, the present work exemplifies the power and efficiency of the HYDROMULTIPOLE simulation package in obtaining high-precision simulation data, for a wide parameter range, of (short-time) transport properties of particles with internal hydrodynamic structure, including highly concentrated suspensions with strong many-body HIs.

ACKNOWLEDGMENTS

G.N., M.L.E.J., and B.C. acknowledge support by the Deutsche Forschungsgemeinschaft (Grant No. SFB-TR6, projects B2 and C1). M.L.E.J. and E.W. were supported in part by the Polish Ministry of Science and Higher Education Grant No. 45/N-COST/2007/0 and the COST P21 Action "Physics of droplets." The work of G.C.A. was supported by CAPES Foundation/Ministry of Education of Brazil. Numerical calculations were carried out at the Academic Computer Center in Gdansk and at the Centre of Excellence BioExploratorium in Warsaw, Poland. M.L.E.J. thanks Dirk van den Ende for helpful discussions.

APPENDIX A: SINGLE-PARTICLE OPERATOR

For a spherical particle, the single-particle friction operator $\mathbf{Z}_0$ is represented by the following matrix:

$$Z_0(ilm\sigma,il'm'\sigma') = \delta_{ll'}\delta_{mm'}\eta(2l+1)\begin{bmatrix} \frac{2l(2l-1)}{l+1}A_{l0} & 0 & (2l-1)(2l+1)A_{l2} \\ 0 & l(l+1)A_{l1} & 0 \\ (2l-1)(2l+1)A_{l2} & 0 & \frac{(l+1)(2l+1)^2(2l+3)}{2l}B_{l2} \end{bmatrix}. \quad \text{(A1)}$$

The scattering coefficients for the two particle models considered in this work are as follows:

(1) Hard sphere of radius a with no-slip boundary conditions:[77]

$$A_{l0} = \frac{2l+1}{2}a^{2l-1}, \quad A_{l1} = a^{2l+1}, \qquad A_{l2} = \frac{2l+3}{2}a^{2l+1}, \quad B_{l2} = \frac{2l+1}{2}a^{2l+3}. \quad \text{(A2)}$$

(2) Uniformly permeable sphere with permeability $1/\kappa^2$:[43]

$$A_{l0} = \frac{2l+1}{2}\frac{g_l(x)}{g_{l-2}(x)}\left[1+\frac{l(2l-1)(2l+1)}{(l+1)x^2}\times\frac{g_l(x)}{g_{l-2}(x)}\right]^{-1}a^{2l-1},$$

$$A_{l1} = \frac{g_{l+1}(x)}{g_{l-1}(x)}a^{2l+1},$$

$$A_{l2} = \left[\frac{2l+3}{2l-1}+\frac{2(2l+1)(2l+3)}{(l+1)x^2}\right]a^2A_{l0}-\frac{2l+3}{2l-1}a^{2l+1},$$

$$B_{l2} = \left[1+\frac{2(2l-1)(2l+1)}{(l+1)x^2}\right]a^2A_{l2}-a^{2l+3}, \quad \text{(A3)}$$

where $x=\kappa a$ and $g_l(x)=\sqrt{\pi/2x}I_{l+1/2}(x)$ is a modified spherical Bessel function of the first kind.

APPENDIX B: FINITE-SIZE CORRECTION

Our simulation data for $H_N(q)$ has been corrected for finite-size effects according to the relation given in Eq. (28). This formula requires as input the structure factor $S(q)$ of nonoverlapping spheres, which has been calculated by using the VW corrected PY expression.[71,72] The functional form of the system size dependence of $H_N(q)$ in Eq. (28) is independent of the particle model, with the effects of the hydrodynamic internal structure of the spheres accounted for by the high-frequency effective viscosity $\eta_{\text{eff}}(x,\phi)$.

In the case of nonpermeable hard spheres, an empirical expression for η_{eff} is available,[22,30]

$$\frac{\eta_{\text{eff}}(\phi)}{\eta_0} = \frac{1+1.5\phi(1+S(\phi))}{1-\phi(1+S(\phi))}, \quad \text{(B1)}$$

with $S(\phi)=\phi+\phi^2-2.3\phi^3$. This expression applies to high concentrations even up to random closed packing.

For permeable particles, the effective viscosity for a very dilute suspension is given by

$$\eta_{\text{eff}}(x,\phi) = \eta_0[1+[\eta](x)\phi+\mathcal{O}(\phi^2)], \quad \text{(B2)}$$

with the expression

$$[\eta](x) = \frac{5}{2}\Omega_v(x) = \frac{5}{2}\left(\frac{G(x)}{1+10G(x)/x^2}\right), \quad \text{(B3)}$$

for the intrinsic viscosity of homogeneously permeable spheres.[17] Here, $G(x)=1+3/x^2-3\coth(x)/x$ so that for large x where $\Omega_v(x\to+\infty)=1$, Einstein's result for the intrinsic viscosity of impermeable spheres is recovered, and $\Omega_v(x\ll 1)\approx x^2/25-2x^4/875$. The function Ω_v is the ratio of the intrinsic viscosities of hard and porous spheres.

For higher volume fractions, we can evaluate the effective viscosity directly by numerical simulations,[69] but only for strongly permeable spheres ($x\leq 10$). Numerical calculations of effective viscosity in the whole range of explored x and ϕ values will be the subject of a future publication. For $x>10$, the ratio $\eta_0/\eta_{\text{eff}}(x,\phi)$ in Eq. (28), which is independent of q, has been evaluated by inspecting the behavior of $H_N(q)$ with the system size, in particular in the infinite-q limit, where $H(q)=D_s/D_0$ and $S(\infty)=1$. Figure 9 displays the size dependence of $H_N(\infty)$ for $x=10$, which agrees with the scaling in Eq. (28). For each x and ϕ, the value $H_N(\infty)$ has been calculated for $N=256$, 512, and 1024. The factor $\eta/\eta_{\text{eff}}(x,\phi)$ was then estimated in terms of the slope of a straight line fitting to the data for $H_N(\infty)$, as a function of

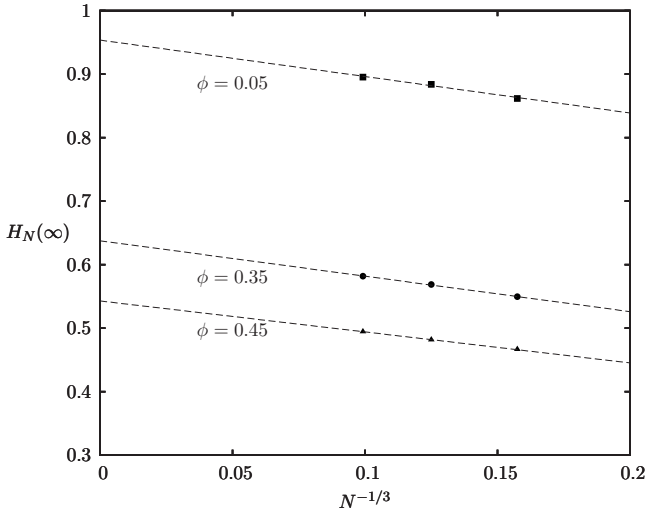

FIG. 9. System-size dependence of the infinite-q limit of $H_N(q)$ for $x=10$ and $\phi=0.05$, 0.35, and 0.45. The uncertainties in $H_N(\infty)$ are smaller than the size of the symbols.

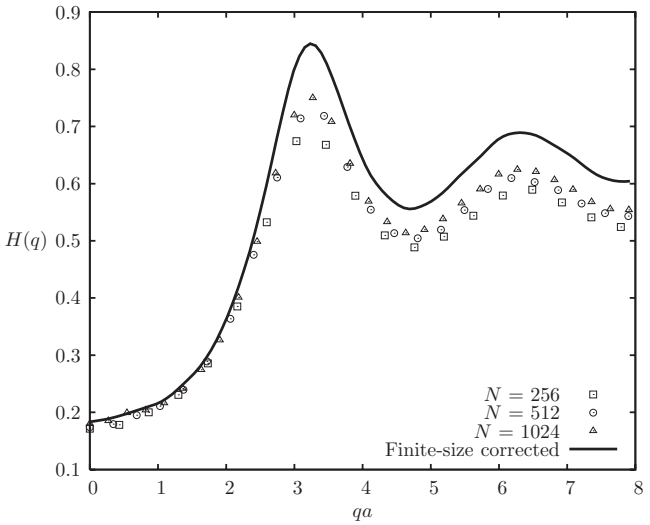

FIG. 10. Finite-size corrected $H(q)$ (continuous line) obtained from $H_N(q)$ using Eq. (28) for $x=10$, $\phi=0.35$, and $N=256$, 512, and 1024 (open symbols).

$N^{-1/3}$. This procedure indirectly produces estimates of the effective viscosity, which are in agreement with the predictions of Eqs. (B1) and (B2), and with directly simulated values of $\eta_{\text{eff}}(x,\phi)$ for $x \leq 10$.

Using Eq. (28) with $S(q)$ and $\eta_{\text{eff}}(x,\phi)$ calculated as described above, we obtain the infinite-system hydrodynamic function $H(q)$. As demonstrated in Fig. 10 for $x=10$ and $\phi=0.35$, the simulation data of $H_N(q)$ obtained for $N=256$, 512, and 1024 collapse on a single master curve when Eq. (28) is used. The master curve is identified as the finite-size corrected form of $H(q)$.

APPENDIX C: LARGE-WAVENUMBER EXTRAPOLATION TO THE SELF-DIFFUSION COEFFICIENT

In this appendix an effective method is presented that allows to deduce D_s/D_0 from data for $H(q)$. Our approach is based on the large-q asymptotic expression for $H(q)$. According to Eq. (7), this asymptotic expression follows from Eq. (6), with the term with $i=j$ excluded from the summation, but with an average calculated partially, i.e., over configurations of all particles, except the pair under consideration. By virtue of the spherical symmetry of the pair mobilities and correlation functions, $H_d(q)$ may be expressed in terms of real and imaginary parts of integrals of the form,

$$\int_{2a}^{+\infty} \mathrm{d}r A(r) e^{iqr}, \tag{C1}$$

where $A(r)$ is a regular function. The large-q analysis of the integral in Eq. (C1) yields (see Ref. 78)

$$H(q) \simeq \frac{D_s}{D_0} + \alpha \frac{\cos y}{y^2} + \beta \frac{\sin y}{y^3} + \cdots, \quad \text{for } y = 2aq \gg 1, \tag{C2}$$

where α and β are parameters depending on ϕ and x. Higher order terms in the asymptotic expansion in Eq. (C2) are of the form $a_{2n}\cos(y)/y^{2n} + a_{2n+1}\sin(y)/y^{2n+1}$, with real-valued coefficients a_{2n} and a_{2n+1} for $n=2,3,\cdots$.

We employ the asymptotic expansion in Eq. (C2) to determine the self-diffusion coefficient. To this end we use the least-squares method to fit a function of form given in Eq. (C2) to the data for $H(q)$ in the interval $4 \leq qa \leq 8$. The self-diffusion coefficient is then determined as one of the fitting parameters.

Figure 11 shows the fit to $H(q)$, for $x=\infty$, in the interval $4 \leq qa \leq 8$. The horizontal dashed (red) lines in Fig. 11 indicate the value of D_s/D_0 determined by direct simulation according to Eq. (8). The horizontal continuous lines represent the infinite-q limit value of $H(q)$ deduced from the fitting procedure. Although the fitting function does not exactly reproduce the shape of $H(q)$ at larger ϕ, an excellent estimate of $H(q \to \infty)$ is obtained which is practically identical to the directly calculated D_s/D_0, with differences smaller than 0.001.

As a final application, we use now the expansion form in Eq. (C2) to justify Pusey's method[24,75] of estimating D_s/D_0 by measuring $H(q)$ at a $q^* > q_m$ where $S(q^*)=1$. One can show that $S(q)$ and $H(q)$ share a similar large-q asymptotic form, so that

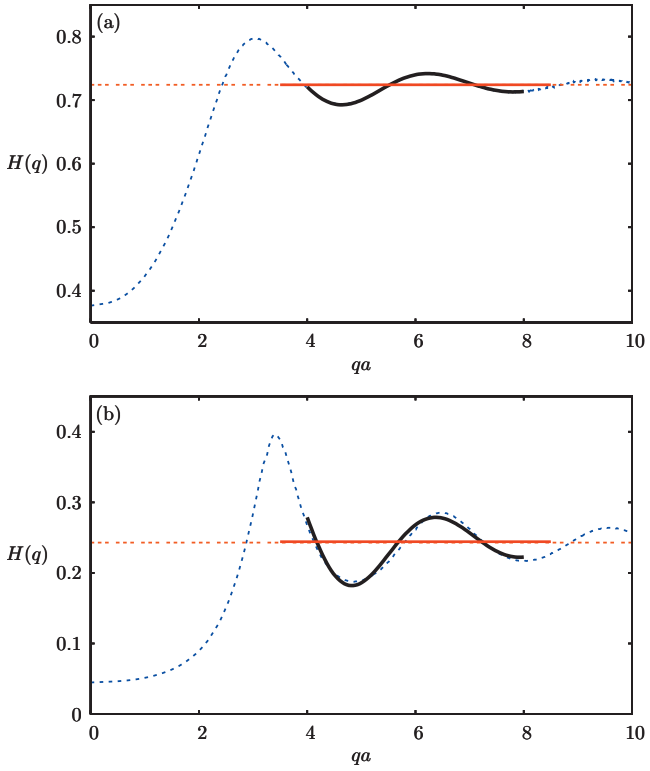

FIG. 11. Fit of the asymptotic form in Eq. (C2) (continuous dark line) to data for $H(q)$ (dashed blue line), for $x=\infty$ and (a) $\phi=0.15$, and (b) $\phi=0.45$. For the fitting procedure, data of $H(q)$ in the interval $4 \leq qa \leq 8$ are used. The horizontal dashed (red) lines give D_s/D_0 determined by direct simulation according to Eq. (8). The horizontal continuous lines represent the infinite-q value of $H(q)$ deduced from the fitting procedure.

$$S(q) \simeq 1 + \alpha' \frac{\cos y}{y^2} + \beta' \frac{\sin y}{y^3} + \cdots, \quad \text{for } y = 2aq \gg 1. \tag{C3}$$

Equation (C3) differs from Eq. (C2) only in the expansion coefficients, in particular in the infinite-q limit where $S(q \to \infty) = 1$. Thus, for a $q^* > q_m$ with $S(q^*) = 1$, it follows from Eq. (C3) that $H(q^*)$ differs from D_s/D_0 by terms of order $1/(aq^*)^3$ only.

[1] T. Eckert and W. Richtering, J. Chem. Phys. **129**, 124902 (2008).
[2] E. Bartsch, V. Frentz, J. Baschnagel, W. Schärtl, and H. Sillescu, J. Chem. Phys. **106**, 3743 (1997).
[3] S. Höfl, L. Zitzler, T. Hellweg, S. Herminghaus, and F. Mugele, Polymer **48**, 245 (2007).
[4] E. H. Purnomo, D. van den Ende, J. Mellema, and F. Mugele, Phys. Rev. E **76**, 021404 (2007).
[5] E. H. Purnomo, D. van den Ende, S. A. Vanapalli, and F. Mugele, Phys. Rev. Lett. **101**, 238301 (2008).
[6] C. A. Coutinho, R. K. Harrinauth, and V. K. Gupta, Colloids Surf., A **318**, 111 (2008).
[7] G. Petekidis, J. Gapinski, P. Seymour, J. S. van Duijneveldt, D. Vlassopoulos, and G. Fytas, Phys. Rev. E **69**, 042401 (2004).
[8] M. Zackrisson, A. Stradner, P. Schurtenberger, and J. Bergenholtz, Phys. Rev. E **73**, 011408 (2006).
[9] M. Zackrisson, A. Stradner, P. Schurtenberger, and J. Bergenholtz, Langmuir **21**, 10835 (2005).
[10] P. A. Nommensen, M. H. G. Duits, J. S. Lopulissa, D. van den Ende, and J. Mellema, Prog. Colloid Polym. Sci. **110**, 144 (1998).
[11] P. A. Nommensen, M. H. G. Duits, D. van den Ende, and J. Mellema, Phys. Rev. E **59**, 3147 (1999).
[12] P. A. Nommensen, M. H. G. Duits, D. van den Ende, and J. Mellema, Langmuir **16**, 1902 (2000).
[13] H. M. Schaink, P. A. Nommensen, R. J. J. Jongschaap, and J. Mellema, J. Chem. Phys. **113**, 2484 (2000).
[14] P. A. Nommensen, D. van den Ende, M. H. G. Duits, and J. Mellema, Langmuir **17**, 5757 (2001).
[15] M. H. G. Duits, P. A. Nommensen, D. van den Ende, and J. Mellema, Colloids Surf., A **183–185**, 335 (2001).
[16] P. Voudouris, J. Choi, H. Dong, M. R. Bockstaller, K. Matyjaszewski, and G. Fytas, Macromolecules **42**, 2721 (2009).
[17] P. Debye and A. M. Bueche, J. Chem. Phys. **16**, 573 (1948).
[18] H.C. Brinkman, Appl. Sci. Res., Sect. A **1**, 27 (1947).
[19] P. Levresse, I. Manas-Zloczower, and D. L. Feke, Chem. Eng. Sci. **56**, 3211 (2001).
[20] L. Raynaud, B. Ernst, C. Verge, and J. Mewis, J. Colloid Interface Sci. **181**, 11 (1996).
[21] A. Weiss, N. Dingenouts, M. Ballauff, H. Senff, and W. Richtering, Langmuir **14**, 5083 (1998).
[22] A. J. C. Ladd, J. Chem. Phys. **93**, 3484 (1990).
[23] A. J. C. Ladd, H. Gang, J. X. Zhu, and D. A. Weitz, Phys. Rev. E **52**, 6550 (1995).
[24] P. N. Segrè, O. P. Behrend, and P. N. Pusey, Phys. Rev. E **52**, 5070 (1995).
[25] O. P. Behrend, Ph.D. thesis, University of Edinburgh, 1995.
[26] A. Sierou and J. F. Brady, J. Fluid Mech. **448**, 115 (2001).
[27] A. J. Banchio and J. F. Brady, J. Chem. Phys. **118**, 10323 (2003).
[28] J. F. Brady, Curr. Opin. Colloid Interface Sci. **1**, 472 (1996).
[29] A. J. Banchio, J. Gapinski, A. Patkowski, W. Häussler, A. Fluerasu, S. Saccana, P. Holmqvist, G. Meier, M. P. Lettinga, and G. Nägele, Phys. Rev. Lett. **96**, 138303 (2006).
[30] A. J. Banchio and G. Nägele, J. Chem. Phys. **128**, 104903 (2008).
[31] J. Gapinski, A. Patkowski, A. J. Banchio, J. Buitenhuis, P. Holmqvist, M. P. Lettinga, G. Meier, and G. Nägele, J. Chem. Phys. **130**, 084503 (2009).
[32] W. B. Russel, D. A. Saville, and W. R. Schowalter, *Colloidal Dispersions* (Cambridge University Press, Cambridge, 1989).
[33] S. B. Chen, Phys. Fluids **10**, 1550 (1998).
[34] P. G. Wolynes and J. A. McCammon, Macromolecules **10**, 86 (1977).
[35] R. M. Wu, H. Y. Chung, and D. J. Lee, Chem. Eng. Sci. **59**, 943 (2004).
[36] S. B. Chen and A. Cai, J. Colloid Interface Sci. **217**, 328 (1999).
[37] G. Mo and A. S. Sangani, Phys. Fluids **6**, 1637 (1994).
[38] A. A. Potanin and W. B. Russel, Phys. Rev. E **52**, 730 (1995).
[39] S. L. Elliott and W. B. Russel, J. Rheol. **42**, 361 (1998).
[40] B. U. Felderhof, Physica A **151**, 1 (1988).
[41] B. Cichocki, B. U. Felderhof, K. Hinsen, E. Wajnryb, and J. Bławzdziewicz, J. Chem. Phys. **100**, 3780 (1994).
[42] M. L. Ekiel-Jeżewska and E. Wajnryb, in *Theoretical Methods for Micro Scale Viscous Flows*, edited by F. Feuillebois and A. Sellier (Transworld Research Network, Kerala, 2009).
[43] R. Reuland, B. U. Felderhof, and R. B. Jones, Physica A **93**, 465 (1978).
[44] R. B. Jones and R. Schmitz, Physica A **149A**, 373 (1988).
[45] B. Cichocki, B. U. Felderhof, and R. Schmitz, PCH, PhysicoChem. Hydrodyn. **10**, 383 (1988).
[46] J. Bławzdziewicz, E. Wajnryb, and M. Loewenberg, J. Fluid Mech. **395**, 29 (1999).
[47] B. Cichocki and B. U. Felderhof, J. Chem. Phys. **130**, 164712 (2009).
[48] S. Kim and S. J. Karrila, *Microhydrodynamics*, (Dover, Mineola, 2005).
[49] P. N. Pusey, in *Liquids, Freezing and the Glass Transition*, edited by J.-P. Hansen, D. Levesque, and J. Zinn-Justin (Elsevier, Amsterdam, 1991), pp. 763–942.
[50] G. Nägele, Phys. Rep. **272**, 215 (1996).
[51] R. B. Jones and P. N. Pusey, Annu. Rev. Phys. Chem. **42**, 137 (1991).
[52] P. Szymczak and B. Cichocki, J. Stat. Mech.: Theory Exp. **2008**, P0125 (2008).
[53] G. Neale, N. Epstein, and W. Nader, Chem. Eng. Sci. **28**, 1865 (1973).
[54] B. U. Felderhof and R. B. Jones, Physica A **93**, 457 (1978).
[55] S. B. Chen and X. Ye, J. Colloid Interface Sci. **221**, 50 (2000).
[56] B. Cichocki, M. L. Ekiel-Jeżewska, and E. Wajnryb, J. Chem. Phys. **111**, 3265 (1999).
[57] B. Cichocki, M. L. Ekiel-Jeżewska, P. Szymczak, and E. Wajnryb, J. Chem. Phys. **117**, 1231 (2002).
[58] R. G. Cox and H. Brenner, J. Fluid Mech. **28**, 391 (1967).
[59] P. Mazur and D. Bedeaux, Physica (Amsterdam) **76**, 235 (1974).
[60] B. U. Felderhof, Physica A **84**, 569 (1976).
[61] R. Schmitz and B. U. Felderhof, Physica A **113**, 90 (1982).
[62] R. Schmitz and B. U. Felderhof, Physica A **113**, 103 (1982).
[63] B. Cichocki, R. B. Jones, R. Kutteh, and E. Wajnryb, J. Chem. Phys. **112**, 2548 (2000).
[64] L. Durlofsky, J. F. Brady, and G. Bossis, J. Fluid Mech. **180**, 21 (1987).
[65] J. F. Brady and G. Bossis, Annu. Rev. Fluid Mech. **20**, 111 (1988).
[66] H. Hasimoto, J. Fluid Mech. **5**, 317 (1959).
[67] B. U. Felderhof, in *Fundamental Problems in Statistical Mechanics VII*, edited by H. van Beijeren (North-Holland, Amsterdam, 1990).
[68] G. H. Golub and C. F. Van Loan, *Matrix Computations* (The Johns Hopkins University Press, Baltimore, 1996).
[69] G. C. Abade, Ph. D. thesis, University of Warsaw, Poland, 2009.
[70] L. Greengard and V. Rokhlin, J. Comput. Phys. **73**, 325 (1987).
[71] L. Verlet and J. J. Weis, Phys. Rev. A **5**, 939 (1972).
[72] W. R. Smith, D. J. Henderson, P. J. Leonard, J. A. Barker, and E. W. Grundke, Mol. Phys. **106**, 3 (2007).
[73] G. K. Batchelor, J. Fluid Mech. **52**, 245 (1972).
[74] P. Szymczak and B. Cichocki, J. Chem. Phys. **121**, 3329 (2004).
[75] P. N. Pusey, J. Phys. A **11**, 119 (1978).
[76] D. O. Riese, G. H. Wegdam, W. L. Vos, R. Sprik, D. Fenistein, J. H. H. Bongaerts, and G. Grübel, Phys. Rev. Lett. **85**, 5460 (2000).
[77] R. Schmitz and B. U. Felderhof, Physica A **92**, 423 (1978).
[78] A. Erdélyi, *Asymptotic Expansions* (Dover, New York, 1987).